ANL/GTRI/TM-13/10

Neutronics Calculations for SPERT-III, E-Core

Nuclear Engineering Division

About Argonne National Laboratory

Argonne is a U.S. Department of Energy laboratory managed by UChicago Argonne, LLC under contract DE-AC02-06CH11357. The Laboratory's main facility is outside Chicago, at 9700 South Cass Avenue, Argonne, Illinois 60439. For information about Argonne and its pioneering science and technology programs, see www.anl.gov.

Availability of This Report

This report is available, at no cost, at http://www.osti.gov/bridge. It is also available on paper to the U.S. Department of Energy and its contractors, for a processing fee, from:

U.S. Department of Energy
Office of Scientific and Technical Information
P.O. Box 62
Oak Ridge, TN 37831-0062
phone (865) 576-8401
fax (865) 576-5728
reports@adonis.osti.gov

ANL/GTRI/TM-13/10

Neutronics Calculations for SPERT-III, E-Core

by
Arne P. Olson
Nuclear Engineering Division, Argonne National Laboratory

May 30, 2013

NEUTRONICS CALCULATIONS for SPERT-III, E-CORE

Arne P. Olson

Nuclear Engineering Division

Argonne National Laboratory

9700 S. Cass Ave.

Argonne, IL 60439 USA

5/30/2013

List of Tables

List of Figures

Fig.22. Comparison of Predictions of Peak Clad Surface Temperature (T-84, T-85, T-86), 533 K, Operating Power, With Flow

Fig.23. Control Rod Reactivity Worth vs. Position

Fig.24. Transient Rod Reactivity Worth vs. Time, for Low-Power Operation at 533 K

Foreword

This work was prepared for the International Atomic Energy Agency under CRP1496 titled "Benchmarking against Experimental Data of the Neutronic and Thermalhydraulic Computational Methods and Tools for Operation and Safety Analysis for Research Reactors." This CRP was first proposed in 2008. The work of the participants will be completed by February 15, 2013.

Introduction and Background

The USA (DOE/NNSA) through Argonne National Laboratory agreed to participate in CRP1496. Specifically, Argonne agreed to prepare a benchmark specification for the SPERT-III reactor experiments that were carried out in the 1960's. It was also agreed that Argonne would conduct an analysis of a selection of those experiments. This report consists of that analysis. The Benchmark Specification document (IAEA CRP: Innovative Methods for Research Reactors, SPERT III E-CORE Reactor Specification, IAEA, 2012), contains descriptions of 9 reactors and associated experiments. It is available from the IAEA.

Description of Tools and Codes

The MCNP5 code used for the analysis was version 1.60, with standard libraries (ENDF-B/VII). It is documented in [1].

PARET is a 1-dimensional point-kinetics code which uses "channels" to represent portions of a reactor that operate at about the same power density. Each channel provides reactivity feedback through temperature and void change of the water coolant, and temperature change in the fuel. Fuel may be in the form of flat plates or rods. Preliminary analyses used version 7.5 of the code [2]. The final results were obtained using version 7.6, dated Sept. 22, 2012 [2].

General Description of SPERT-III E-Core

Detailed Specifications are given in the companion document: IAEA CRP: Innovative Methods for Research Reactors, SPERT III E-CORE Reactor Specification, IAEA, 2012. This Specification was derived mainly from SPERT-III reports [3, 4].

The E-core of the SPERT-III reactor that is analyzed herein consists of a 60-assembly loading. There are 8 control rods in 4 pairs, and a centrally located transient rod. Twelve assemblies are of the 16-rod type and 52 are of the 25-rod type. The fuel is uranium oxide pellets clad in stainless-steel pins, of low-enriched (4.80%) uranium, contained in stainless-steel fuel assemblies. There are 1492 fuel pins with a total Uranium mass of 1200.6 kg (57.6 kg U-235).

Experimental Program

The E-core experimental program [4] was divided into low-initial-power and high-initial-power test phases. Low-initial-power (≈50 W) excursions were performed for cold- and hot-startup conditions. High-initial-power excursions were performed for hot-standby and operating-power conditions. For the E-core, these system conditions are defined as:

Accident Conditions	Coolant Inlet Temperature	Initial Reactor Power (MW)
Cold Startup	70 °F / 21 °C	$5x10^{-5}$
Hot Startup	260 °F / 127 °C	$5x10^{-5}$
	500 °F / 260 °C	$5x10^{-5}$
Hot Standby	500 °F / 260 °C	1
Operating Power	500 °F / 260 °C	20

With the exception of the cold-startup excursions, the test conditions were generally 1500 psig (10.34 MPa) system pressure and 14 fps (4.267 m/s) coolant velocity along the fuel rods. With respect to coolant pressure, velocity, and subcooling, and to specific core power, the initial test conditions were characteristic of commercial PWR operating conditions. Cold-startup was unpressurized at local atmospheric pressure (approximately 1500 m altitude) and zero flow.

Cold-Startup Accident test conditions are summarized in Table 1. Hot-Startup Accident test conditions are summarized in Table 2. Table 3 is a data summary for hot-standby and operating-power test conditions. Reactor kinetics parameters are needed for conditions that existed for each test series. They are given in Tables 4a, 4b, 5a, 5b, 6a, and 6b.

The analyst has a choice of selecting how to model the initial conditions for each test. It is impractical, for a given test series, to account for the relatively small movement of the control rod bank needed to accommodate a given reactivity insertion, regarding its effect on power shape. It is also better to model and analyse the power shape that exists at the end of the transient rod ejection when the reactor is super-critical. For these tests this amount is about 1 $, which is the average reactivity inserted by ejection of the transient rod. Table 7 provides details of the test series reactivity calculations for that point in time, for each test series.

Table 1. Data Summary for Cold-Startup Accident Tests

Test no.	Period ms	Reac-tivity Inser-tion $	Initial Primary Cool. Temp.	Peak Power MW	Energy Release to Time of Peak Power MW-s	Time to Peak Power s	Max. Measured Clad Surface Temp. Rise†	Reactivity Compensation at Peak Power $
22	1010± 20	0.77± 0.04	74± 4°F 23± 2°C	2.1±0.3	6.9±1.2	13.7±0.2	92±9°F / 51±5°C	0.26±0.03
18	351±7	0.90± 0.04	70± 4°F 21± 2°C	4.3±0.6	6.7±1.1	5.3±0.1	99±10°F / 55±6°C	0.23±0.03
13	206 ± 4	0.93± 0.04	63± 4°F 17± 2°C	5.6±0.8	5.1±0.9	3.2±0.06	127 ±13°F / 71 ±7°C	0.19±0.02
14	195± 4	0.94± 0.04	64± 4°F 18± 2°C	5.6±0.8	5.3±0.9	3.2±0.06	104 ±10°F / 58 ±6°C	0.20±0.02
39	113± 2	0.97± 0.04	65± 4°F 18± 2°C	8.1±1.2	4.7±0.8	1.77±0.07	143± 14°F / 79± 8°C	0.17±0.02
23	111± 2	0.97± 0.04	70± 4°F 21± 2°C	7.7±1.2	4.2±0.7	1.81±0.05	131±13°F / 73±7°C	0.16±0.02
45	96.8±1.9	0.98± 0.04	80± 4°F 27± 2°C	8.2±1.2	3.6±0.6	1.60±0.09	150±15°F / 83±8°C	0.13±0.01
15	95.8± 1.9	0.99± 0.04	66± 4°F 19± 2°C	8.0±1.2	3.4±0.6	1.57±0.01	125 ±13°F / 69 ±7°C	0.13±0.01
50	95.7± 1.9	0.98± 0.04	82± 4°F 28± 2°C	9.2±1.4	3.3±0.6	1.47±0.04	150 ±15°F / 83 ±8°C	0.11±0.01
44	95.2± 1.9	0.98± 0.04	77± 4°F 25± 2°C	8.3±1.2	3.8±0.6	1.55±0.03	132±13°F / 73±7°C	0.14±0.01
46	94.0± 1.9	0.98± 0.04	69± 4°F 21± 2°C	8.5±1.3	4.0±0.6	1.55±0.06	149±15°F / 83±8°C	0.15±0.02
71	94.0± 1.9	0.98± 0.04	92± 4°F 33± 2°C	7.9±1.2	3.6±0.6	1.54±0.06	148±15°F / 82±8°C	0.14±0.01
17	91.0± 1.8	0.99± 0.04	68± 4°F 20± 2°C	8.6±1.3	3.3±0.6	1.20±0.05	117±12°F / 65±7°C	0.12±0.01
74	89.0± 1.8	0.99± 0.04	67± 4°F 19± 2°C	8.9±1.3	3.1±0.5	1.36±0.04	143±14°F / 79±8°C	0.12±0.01

Table 1. Data Summary for Cold-Startup Accident Tests (continued)

Test no.	Period ms	Reac-tivity Inser-tion $	Initial Primary Cool. Temp.	Peak Power MW	Energy Release to Time of Peak Power MW-s	Time to Peak Power s	Max. Measured Clad Surface Temp. Rise†	Reactivity Compensation at Peak Power $
87	87.0± 1.7	0.99± 0.04	66± 4°F 19± 2°C	9.1±1.4	3.8±0.6	1.35±0.04	187±19°F / 104±11°C	0.11±0.01
73	83.0± 1.6	0.99± 0.04	67± 4°F 19± 2°C	8.8±1.3	3.0±0.5	1.40±0.04	150±15°F / 83±8°C	0.13±0.01
51	72.3± 1.4	1.00± 0.04	82± 4°F 28± 2°C	11±2	2.4±0.4	1.08±0.02	130±13°F / 72±7°C	0.09±0.01
49	68.4± 1.4	1.00± 0.04	76± 4°F 24± 2°C	11±2	2.1±0.4	0.97±0.04	142±14°F / 79±8°C	0.08±0.01
16	59.3± 1.2	1.01± 0.04	67± 4°F 19± 2°C	12±2	2.0±0.3	0.86±0.01	118±12°F / 66±7°C	0.08±0.01
38	55.5± 1.1	1.02± 0.04	56± 4°F 13± 2°C	15±2	2.1±0.4	0.79±0.02	166±17°F / 92±9°C	0.07±0.01
19	44.0± 0.9	1.03± 0.04	69± 4°F 21± 2°C	18±3	1.9±0.3	0.63±0.01	115±12°F / 64±7°C	0.07±0.01
20	35.0± 0.7	1.03± 0.04	72± 4°F 22± 2°C	26±4	2.0±0.3	0.54±0.01	123±12°F / 68±7°C	0.08±0.01
75	33.0± 0.7	1.05± 0.04	68± 4°F 20± 2°C	31±5	2.1±0.4	0.50±0.02	152±15°F / 84±8°C	0.08±0.01
21	22.3± 0/4	1.09± 0.04	72± 4°F 22± 2°C	56±8	2.8±0.5	0.38±0.01	118±12°F / 66±7°C	0.11±0.01
40	22.0± 0.4	1.09± 0.04	67± 4°F 19± 2°C	59±9	2.8±0.5	0.39±0.01	158±16°F / 88±9°C	0.11±0.01
48	21.1± 0.4	1.09± 0.04	74± 4°F 23± 2°C	63±9	2.8±0.5	0.37±0.01	141±14°F / 78±8°C	0.11±0.01

Table 1. Data Summary for Cold-Startup Accident Tests (continued)

Test no.	Period ms	Reac-tivity Inser-tion $	Initial Primary Cool. Temp.	Peak Power MW	Energy Release to Time of Peak Power MW-s	Time to Peak Power s	Max. Measured Clad Surface Temp. Rise†	Reactivity Compensation at Peak Power $
42	12.6± 0.3	1.17± 0.05	78± 4°F 26± 2°C	170±26	4.6±0.8	0.250±0.006	147±15°F / 82±8°C	0.18±0.02
43	10.0± 0.2	1.21± 0.05	78± 4°F 26± 2°C	280±42	6.0±1.0	0.23±0.006	148±15°F / 82±8°C	0.22±0.02

† Estimated standard deviation is 10% for measured clad surface temperature rise.

Standard deviation in Power estimated at 15%; in energy to peak power at 17%

Table 2. Data Summary for Hot-Startup Accident Tests

Test no.	Period ms	Reac-tivity Inser-tion $	Initial Primary Cool. Temp.	Flow Rate fps	Peak Power MW	Energy Release to Time of Peak Power MW-s	Time to Peak Power s	Max. Measured Clad Surface Temp. Rise†	Reactivity Compensation at Peak Power $
24	1140 ± 20	0.75± 0.03	259± 4°F 126± 2°C	14	3.0±0.5	16±2.7	18.0±0.1	13±1°F / 7±1°C	0.35±0.04
25	1090 ± 20	0.76± 0.03	259± 4°F 126± 2°C	14	2.8±0.4	8.9±1.5	14.9±0.1	8±1°F / 4±1°C	0.22±0.03
36	249± 5	0.92± 0.04	259± 4°F 126± 2°C	22	6.2±0.9	9.0±1.5	4.5±0.2	21±2°F / 12±1°C	0.25±0.02
26	209± 4	0.93± 0.04	259± 4°F 126± 2°C	14	6.8±1.0	7.6±1.3	3.6±0.1	24±2°F / 13±1°C	0.22±0.02
30	118± 2	0.97± 0.04	259± 4°F 126± 2°C	2.4	7.8±1.2	4.8±0.8	1.98±0.05	66±7°F / 37±4°C	0.15±0.02
37	108± 2	0.98± 0.04	259± 4°F 126± 2°C	19	8.9±1.3	5.7±1.0	1.9±0.1	22±2°F / 12±1°C	0.18±0.02
33	103± 2	0.98± 0.04	259± 4°F 126± 2°C	22	9.4±1.4	5.1±0.9	1.7±0.1	28±3°F / 16±2°C	0.16±0.02
27	102± 2	0.98± 0.04	259± 4°F 126± 2°C	14	9.1±1.4	4.3±0.7	1.6±0.05	26±3°F / 14±2°C	0.14±0.02

Table 2. Data Summary for Hot-Startup Accident Tests (continued)

Test no.	Period ms	Reac-tivity Inser-tion $	Initial Primary Cool. Temp.	Flow Rate fps	Peak Power MW	Energy Release to Time of Peak Power MW-s	Time to Peak Power s	Max. Measured Clad Surface Temp. Rise†	Reactivity Compensation at Peak Power $
35	87.0±1.7	0.99±0.04	259±4°F 126±2°C	22	9.8±1.5	4.1±0.7	1.4±0.1	28±3°F / 16±2°C	0.14±0.02
34	69.9±1.4	1.00±0.04	259±4°F 126±2°C	22	11±2	3.2±0.5	1.17±0.03	25±3°F / 14±2°C	0.11±0.01
28	41.6±0.8	1.03±0.04	259±4°F 126±2°C	14	22±3	2.0±0.3	0.64±0.01	31±3°F / 17±2°C	0.08±0.01
31	39.6±0.8	1.04±0.04	259±4°F 126±2°C	2.4	23±3	2.0±0.3	0.60±0.02	88±9°F / 49±5°C	0.08±0.01
32	21.8±0.4	1.09±0.04	259±4°F 126±2°C	2.4	66±10	3.1±0.5	0.39±0.01	103±10°F / 57±6°C	0.11±0.01
29	19.6±0/4	1.10±0.04	259±4°F 126±2°C	14	78±12	3.2±0.5	0.36±0.01	44±4°F / 24±2°C	0.12±0.01
70	10.3±0.2	1.21±0.05	251±4°F 122±2°C	14	280±42	6.3±1.1	0.20±0.01	58±6°F / 32±3°C	0.22±0.02
12	2260 ± 50	0.64±0.03	500±4°F 260±2°C	14	0.14±0.01	0.45±0.06	20±0.1	≈0 °F / 0°C	0.06±0.01

Table 2. Data Summary for Hot-Startup Accident Tests (continued)

Test no.	Period ms	Reac-tivity Inser-tion $	Initial Primary Cool. Temp.	Flow Rate fps	Peak Power MW	Energy Release to Time of Peak Power MW-s	Time to Peak Power s	Max. Measured Clad Surface Temp. Rise†	Reactivity Compensation at Peak Power $
53	1060 ± 20	0.77± 0.03	500± 4°F 260± 2°C	14	4.0±0.4	14±2	15±0.1	10±1°F / 6±1°C	0.27±0.03
63	592± 10	0.84± 0.03	501± 4°F 261± 2°C	14	5.6±0.6	15±2	9.2±0.2	21±2°F / 12±1°C	0.29±0.03
64	585± 10	0.82± 0.03	501± 4°F 261± 2°C	4.8	4.8±0.5	12±2	8.8±0.2	41±4°F / 23±2°C	0.29±0.03
65	440± 9	0.87± 0.03	500± 4°F 260± 2°C	24	6.6±0.7	13±2	7.0±0.2	13±1°F / 7±1°C	0.26±0.03
54	223± 4	0.93± 0.04	498± 4°F 259± 2°C	14	8.7±0.9	11±1	3.8±0.1	17±2°F / 9±1°C	0.24±0.03
55	70.2± 1. 4	1.00± 0.04	500± 4°F 260± 2°C	14	16±2	3.3±0.4	1.00±0.03	19±2°F / 11±1°C	0.08±0.01
56	37.9± 0.8	1.04± 0.04	501± 4°F 261± 2°C	14	35±4	3.1±0.4	0.62±0.00 7	26±3°F / 14±2°C	0.08±0.01
57	21.7± 0.4	1.09± 0.04	500± 4°F 260± 2°C	14	89±9	4.4±0.6	0.400±0.0 05	31±3°F / 17±2°C	0.12±0.01

Table 2. Data Summary for Hot-Startup Accident Tests (continued)

Test no.	Period ms	Reac-tivity Inser-tion $	Initial Primary Cool. Temp.	Flow Rate fps	Peak Power MW	Energy Release to Time of Peak Power MW-s	Time to Peak Power s	Max. Measured Clad Surface Temp. Rise†	Reactivity Compensation at Peak Power $
62	20.6±0.4	1.10±0.04	500±4°F 260±2°C	14	97±10	4.5±0.6	0.370±0.005	30±3°F / 17±2°C	0.12±0.01
61	17.8±0.4	1.12±0.04	500±4°F 260±2°C	14	120±11	4.9±0.6	0.335±0.005	32±3°F / 18±2°C	0.14±0.02
68	16.0±0.3	1.13±0.05	500±4°F 260±2°C	14	160±16	5.5±0.7	0.300±0.005	33±3°F / 18±2°C	0.15±0.02
67	15.5±0.3	1.14±0.05	501±4°F 261±2°C	4.8	170±17	5.6±0.7	0.300±0.005	60±6°F / 33±3°C	0.16±0.02
66	14.3±0.3	1.15±0.05	500±4°F 260±2°C	24	190±19	5.8±0.8	0.290±0.005	24±2°F / 13±1°C	0.17±0.02
58	14.1±0.3	1.15±0.05	500±4°F 260±2°C	14	200±20	6.2±0.8	0.285±0.005	36±4°F / 20±2°C	0.17±0.02

† Estimated standard deviation is 10% for measured clad surface temperature rise.

Standard deviation in Power estimated at 10%; in energy to peak power at 13% for a system temperature of 500 F.

Table 3. Data Summary for Hot-Standby and Operating-Power Reactivity Accident Tests

Test no.	Reactivity Insertion $	Initial Primary Cool. Inlet Temp.	Flow Rate fps	Initial Reactor Power MW	Peak Reactor Power	Net Energy Release [a] to Time of Peak Power MW-s	Time to Peak Power s	Max. Measured Clad Surface Temp. Rise	Reactivity [b] Compensation at Peak Power $
79	0.86± 0.03	513± 4°F 267± 2°C	14	1.1±0.1	13±1	6.7±0.9	0.68±0.08	510±10°F / 283±6°C	0.09
80	1.08±0.04	506± 4°F 263± 2°C	14	1.3±0.1	120±10	4.5±0.6	0.150±0.003	530±10°F / 294±6°C	0.11
81	1.17± 0.04	514± 4°F 268± 2°C	14	0.9±0.1	330±30	7.8±1	0.135±0.003	540±10°F / 300±6°C	0.18
83	1.25± 0.04	504± 4°F 262± 2°C	14	1.1±0.1	620±60	11±1	0.117±0.002	540±10°F / 300±6°C	0.26
82	1.29± 0.04	505± 4°F 263± 2°C	14	1.2±0.1	880±90	15±2	0.118±0.002	550±10°F / 306±6°C	0.30
84	0.46± 0.02	505± 4°F 263± 2°C	14	19±1	39±4	4.7±0.6	0.18±0.02	590±10°F / 328±6°C	0.03
85	0.87± 0.04	503± 4°F 262± 2°C	14	19±1	130±10	14±2	0.155±0.005	590±10°F / 328±6°C	0.04

Table 3. Data Summary for Hot-Standby and Operating-Power Reactivity Accident Tests (continued)

Test no.	Reactivity Insertion $	Initial Primary Cool. Inlet Temp.	Flow Rate fps	Initial Reactor Power MW	Peak Reactor Power	Net Energy Release [a] to Time of Peak Power MW-s	Time to Peak Power s	Max. Measured Clad Surface Temp. Rise	Reactivity [b] Compensation at Peak Power $
86	1.17± 0.05	502± 4°F 261± 2°C	14	19±1	610± 60	17±2	0.110 ±0.005	600±10°F / 333±6°C	0.22

[a] Incremental energy released during burst above that resulting from steady state operation.

[b] Because of uncertainties in initial reactivity insertions and peak power times, these values are only approximate.

Estimated standard deviation for other measured parameters

- Reactor period 2 %
- Reduced prompt neutron generation time 2.5 %
- Delayed neutron parameters 7-15 %
- Derived reactivity insertion 4 %
- Reactivity compensation at peak power 11 %
- Clad surface temperature rise 10 %

The MCNP Model

The MCNP5 code used for the analysis was version 1.60, with standard libraries (ENDF-B/VII). It is documented in [1].

The radial reactor geometry included all of the radial shields of the facility. The axial model spanned the lower axial reflector, lower grid, core, upper grid, and upper axial reflector. The MCNP code was used for all static computations of reactivity, kinetics parameters for delayed neutrons, and power shape. Kinetics parameters (β_{eff}, l_p, β_i, λ_i) were obtained from MCNP from a user input option (kinetics=yes, precursor=yes). The reactor core contained 60 fuel elements, most of which were of 5x5 type. Others contained 4x4- type for the Transient Rod, and as followers for the Control Rods. The reactor core was modeled with 5 separate types of "universes." Doppler and water temperature coefficients were derived by increasing the UO2 temperature (for Doppler), or by increasing the water temperature (in the core only). In order to obtain the reactivity for a given UO2 temperature, three changes were made. First, the S(α,β) thermal cross sections for Oxygen in UO2 and Uranium-238 in UO2 were changed to the new desired temperature, by selecting the corresponding "ZAID" listed in Appendix G, MCNP Data Libraries. Second, the actual temperature for the uranium oxide pellet composition was changed to that same temperature (on the MTn card). Third, the neutron cross sections to be used above thermal energies were changed by selecting the appropriate identifier (ZAID) for the desired temperature. For water density, a 5% water density reduction was used to obtain the void coefficient.

Direct heating to the moderator (from gamma energy deposition, and from neutron scattering) was not calculated by the MCNP model. Instead, a value of 2.6% was assumed as typical of a PWR UO2 fuel rod [5]. Subsequent PARET calculations for experiment T-86 confirmed that direct heating was significant through more rapid heatup of the coolant. As a result, experiments T-79 through T-86 were recomputed using direct heating. The other cases assumed no direct heating, because the coolant temperature rise in those tests was so small as to make negligible the effect of direct heating. Clad material specifications were obtained from Ref. [6]. The lower and upper grid specifications came from Ref. [7]. Type-304 and Type 304L steel composition was taken from Ref. [8]. Lead brick shielding was assumed to conform to the ASTM Specification B29 [9]. Additional information about flow calculations is available in [10]. It was not needed for this work. A related E-core is described in [11].

The experiments were conducted by reconfiguring the transient rod and control rod locations such that rapid removal of the transient rod from a critical configuration would insert the desired step reactivity. The first step was to insert the transient rod absorber section from below the core to achieve a certain desired subcritical reactivity. Then the control rods were raised, introducing more fuel and less absorber, to achieve a new critical position. Then the transient rod could be rapidly ejected during the test. There is a steel follower above the transient rod absorber section which is inserted fully into the core when the absorber section is fully withdrawn.

Modeling of the control rod assembly was problematic because of lack of actual drawings. The key issue was the lack of detailed dimensions for the region at the top of the 4x4 fuel rod portion of the fueled section. There was an isometric view of the 'control rod,' without dimensions. There are 4 "control rods," ganged together in pairs. There also was information about the fuel rods that there was a gas gap above the meat 6.35 cm in length. And there was information about some additional poison plates in

small pieces located between the upper absorber section and the 4x4 rodded section, inside the upper end of the normal steel box surrounding the 4x4 pins. This additional poison material in small plates was placed inside the end of the 4x4 normal steel boxes, apparently to cover the 6.35 cm gas gap region. As a result, the key uncertainty concerns the location of the top of the fuel meat. It was assumed that the upper poisoned section terminated at the top of the meat. The top of the control rod meat was located at -11.557 – 6.35 cm (-4.55 -2.50 in.) for the "cold" 293 K cases. The 400 K cases were modeled by shifting the control rod meat to -15.80 cm in order to account for negative feedbacks at that temperature. The 533 K cases (at power) cases were modeled by shifting the control rod meat to +5.70 cm in order to account for negative feedbacks at that temperature. As a consequence, three different power profiles, kinetics parameters, and feedback coefficients were obtained to represent test conditions at 293 K, 400 K, and 533 K.

The available excess reactivity at 300 K and at 533 K is quoted [4] as ~14 $ and ~4.7 $. It is not known what uncertainty applies to these values. Also not known is how they were determined. The present calculation values are 12.66 $ and 6.0 $ at 300 K and 533 K.

The transient rod is quoted [4] as having a worth of ~4.8 $ at 300 K, and 3.5 $ at 533 K. The present calculated value is 6.0 $ at 300 K.

The PARET Model and its Relationship to the MCNP Model

Fig.1 illustrates how the core loading was grouped into MCNP "Universes". The purpose of this grouping was to take advantage of the symmetries in the core loading caused by the position of the transient rod and control rods.

```
 1  1  1  1  1  1  1  1  1  1  1  1  1  $ROW 1
 1  1  1 11 11 11 11 11 11  1  1  1  1  $ROW 2
 1  1 11 11 11 11 11 11 11 11  1  1  1  $ROW 3
 1 11 11 10 10 10 10 10 10 11 11  1  1  $ROW 4
11 11 10  2  2  4  2  2  2 10 11 11  1  $ROW 5
11 11 10  2  4  9  9  4  2 10 11 11  1  $ROW 6
11 11 10  2  9  7  8  9  4 10 11 11  1  $ROW 7
11 11 10  4  9  6  5  9  2 10 11 11  1  $ROW 8
11 11 10  2  4  9  9  4  2 10 11 11  1  $ROW 9
11 11 10  2  2  2  4  2  2 10 11 11  1  $ROW 10
 1 11 11 10 10 10 10 10 10 11 11  1  1  $ROW 11
 1  1 11 11 11 11 11 11 11 11  1  1  1  $ROW 12
 1  1  1 11 11 11 11 11 11  1  1  1  1  $ROW 13
```

Universe Number	Description
2	16 outer fuel assemblies with 5x5
4	8 Control Rod assemblies with 4x4
5, 6, 7, 8	Central 4 around Transient Rod with 4x4
9	Next most central 8 fuel with 5x5
10	Next 24 fuel with 5x5
11	Water + channel box
1	Water +channel box

Fig.1. Universe Map in MCNP Model of 60-Element Core

Figs. 2 and 3 show details of the geometry in the MCNP model, for a horizontal plane through the axial core center.

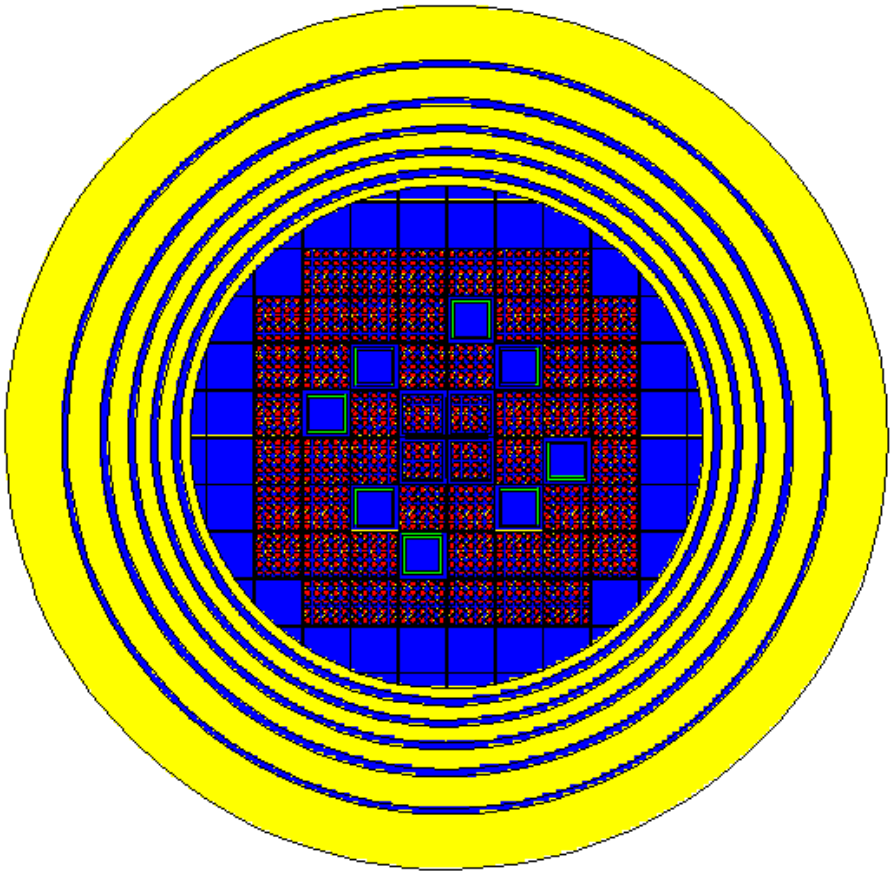

Fig. 2. SPERT-III Reactor E-Core, MCNP Model, at the Axial Mid-Plane

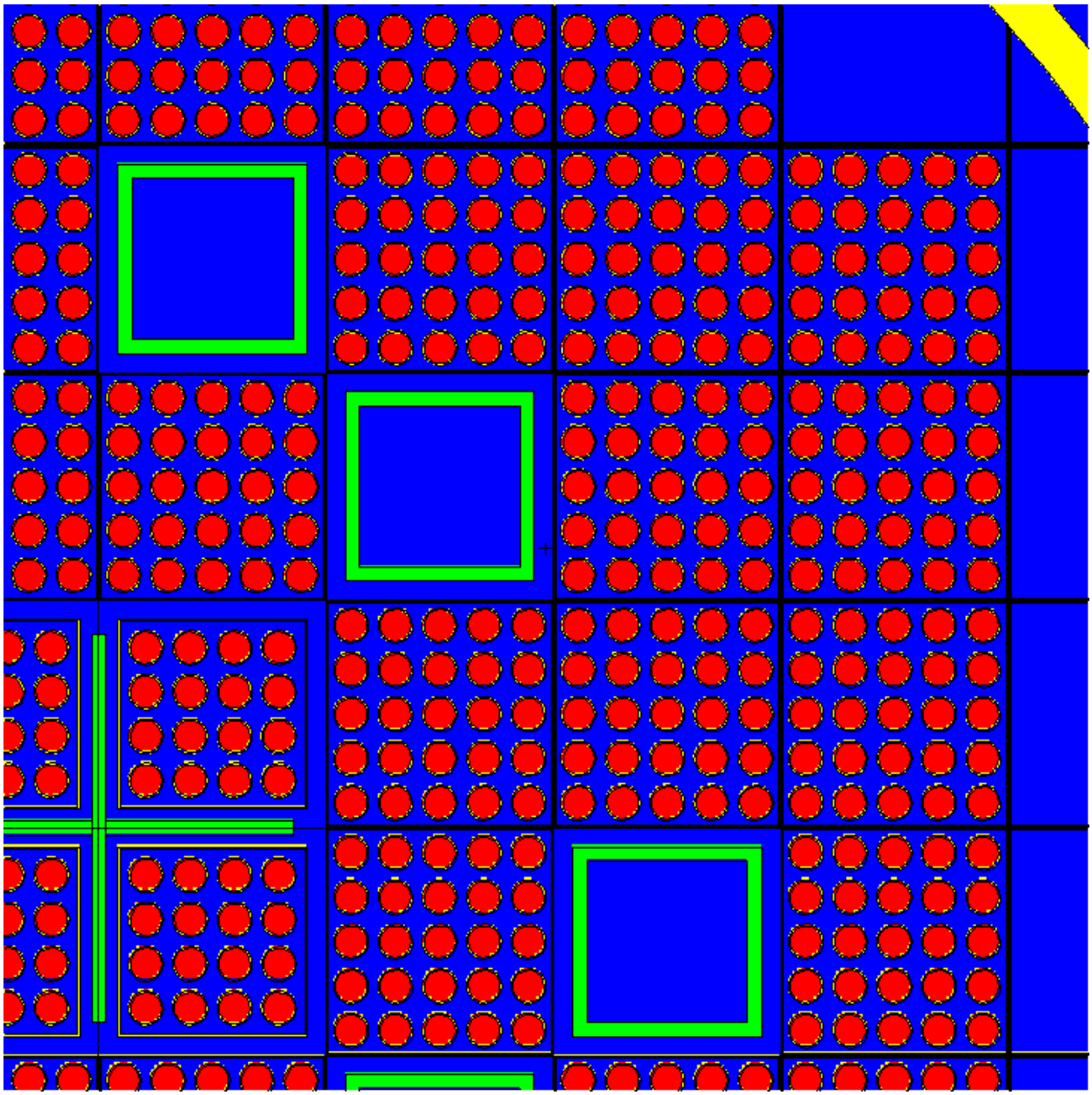

Fig.3. Enlargement of SPERT-III Reactor E-Core, MCNP Model, at the Axial Mid-Plane

At minimum, a 2-channel model is needed by PARET in order to represent a core. In such a model, the "peak" channel would represent the channel with the highest power density, and the "average" channel would represent every other channel. Note that the "average" channel is not quite the average of the whole core: it is just the average of everything in the core except the "peak" channel. Because of these symmetries Universes 2, 4, (5-8), 9, and 10 became separate "channels" in the 5-channel PARET model. Universe 11 contained only the channel box. The core fractions the each channel represented were based on the number of channels containing fuel in each universe. The axial fission rate for each universe was tallied in MCNP for 20 equal-length axial segments. These relative rates were normalized to a core average power of 1, and supplied to PARET. The PARET mode therefore accounted for the spatial power distribution both radially and axially, within the limits of 5 channels, each with 20 axial modes. The normalized axial flux profiles in the 5 channels are shown in Figs. 4-6.

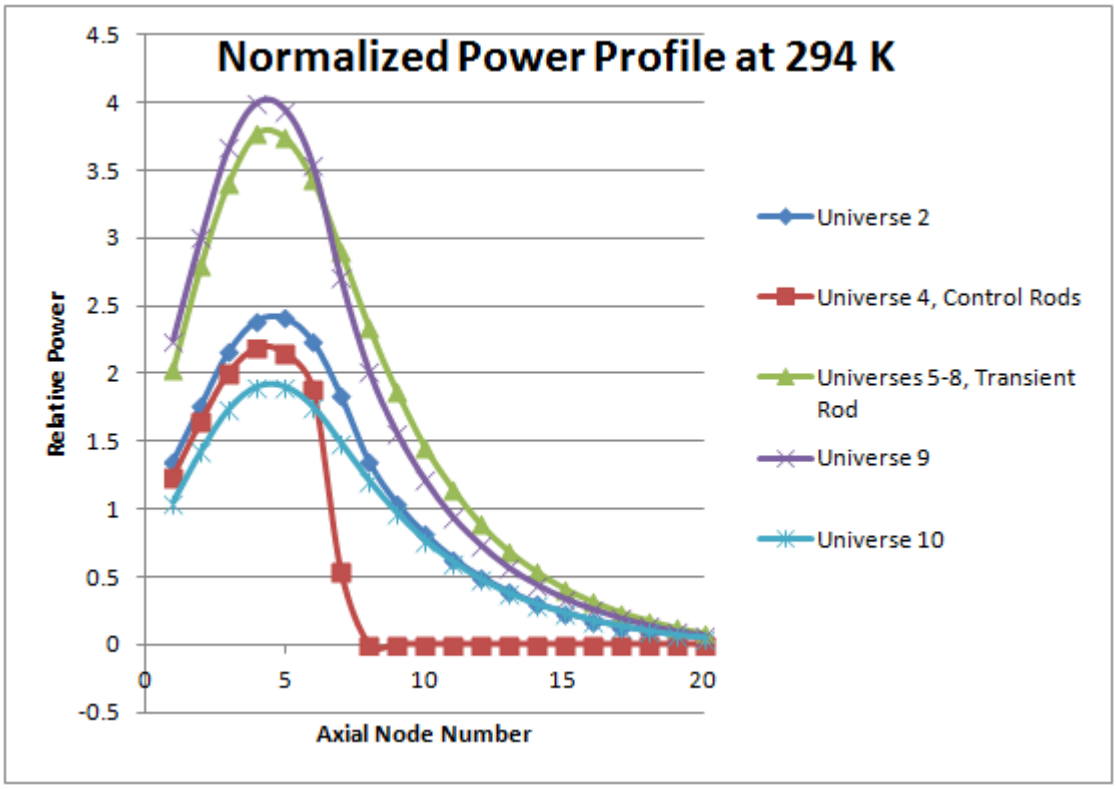

Fig.4. Normalized Power Profiles by Channel and Axial Node, at 294 K

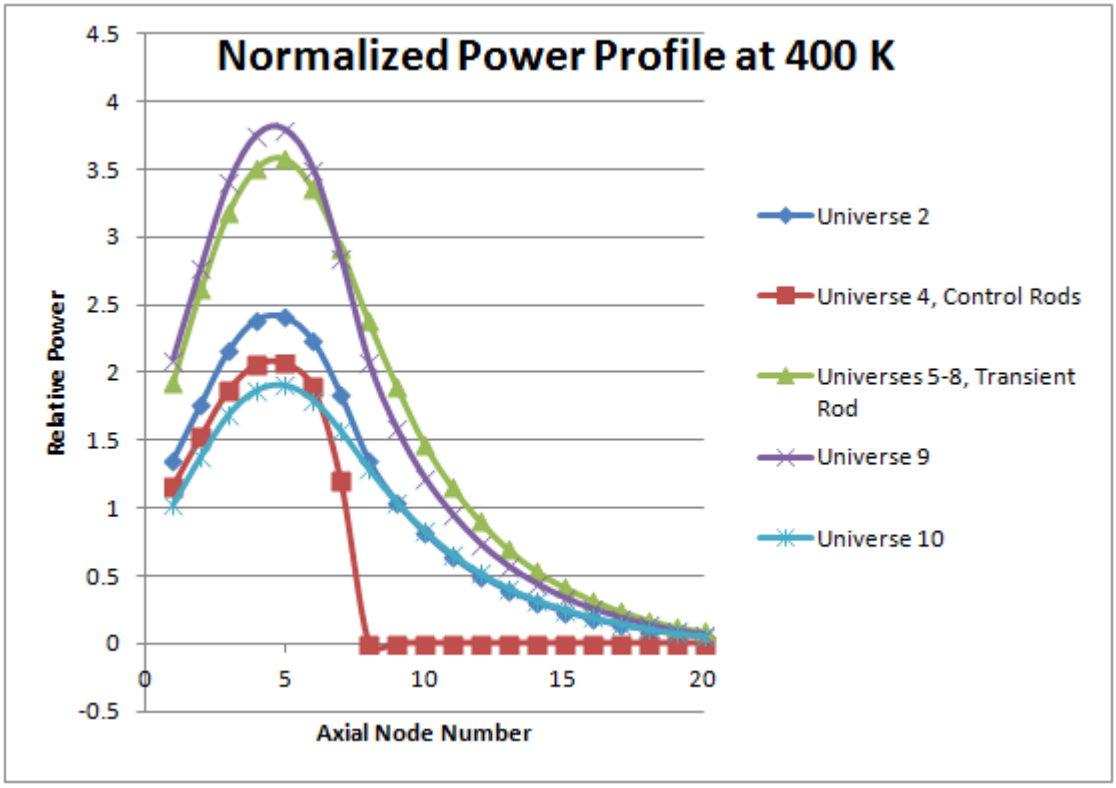

Fig.5. Normalized Power Profiles by Channel and Axial Node, at 400 K

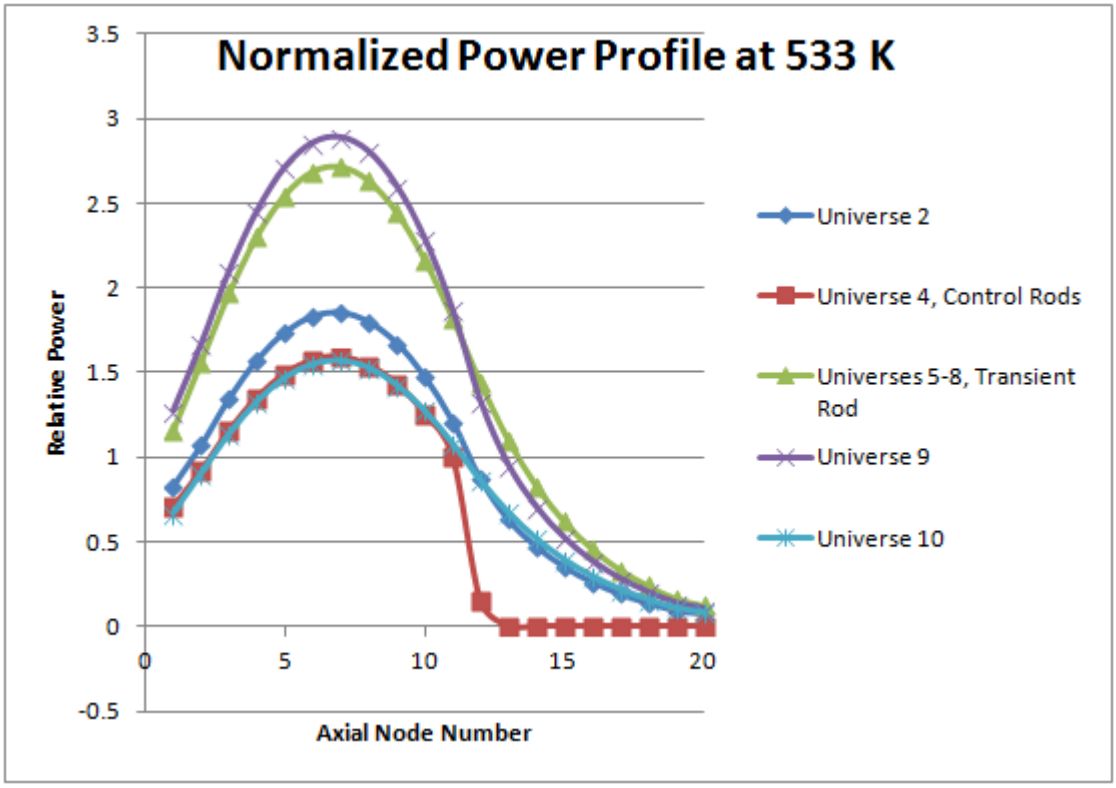

Fig.6. Normalized Power Profiles by Channel and Axial Node, at 533 K

The PARET model of a "channel" consisted of a cylindrical unit cell: fuel rod, gap, and clad surrounded by water. This unit cell model was used for cold tests. For the hot Tests at 19 MW and 533 K, it was assumed that the gap was closed up (consistent with [4], for operating power conditions). Details of geometry and materials also came from [6-10].

The PARET code can utilize space-dependent weighting of reactivity feedback effects from Doppler, coolant temperature change, and coolant density change (void). However, it is a very complex problem to actually calculate what those 3D spatial weighting effects might be. For the purposes of this CRP, it is a reasonable approximation to assume that the spatial weighting can be ignored. In other words, it is set to 1.0 for all spatial volumes in the PARET model. As a result, one can expect to under-predict the Doppler Effect in the hottest fuel, and to under-predict the temperature feedback effect of the hottest coolant in the exit half of any channel. So the calculations can be expected to be "bounding" with regard to key results such as peak power, energy release at time of peak power, and peak clad temperature.

Reactivity kinetics parameters β_{eff}, neutron generation time, and 6-delayed-group parameters β_i and λ_i came from MCNP calculations at the three reference conditions of temperature and pressure. Tables 4a, 4b, 5a, 5b, 6a, and 6b provide these point-kinetics parameters.

Table 4a. Kinetics Parameters for Cold Startup (294 K)

Coolant Inlet Temp., K	Effective Delayed Neutron Fraction, β_{eff}	Prompt Neutron Generation Time λ, μs
294	0.00778 ± 0.00021	17.720 ± 0.06

Table 4b. Delayed Neutrons for Cold Startup (294 K)

Delayed Neutron Group	Fraction, β_i	Decay Constant, 1/s
1	0.00018	0.01249
2	0.00122	0.03166
3	0.00113	0.11012
4	0.00370	0.32041
5	0.00121	1.34624
6	0.00035	8.87246

Table 5a. Kinetics Parameters for Hot Startup (400 K)

Coolant Inlet Temp., K	Effective Delayed Neutron Fraction, β_{eff}	Prompt Neutron Generation Time λ, μs
394	0.00759 ± 0.00021	18.007 ± 0.06

Table 5b. Delayed Neutrons for Hot Startup (400 K)

Delayed Neutron Group	Fraction, β_i	Decay Constant, 1/s
1	0.00020	0.01249
2	0.00105	0.03166
3	0.00131	0.11015
4	0.00354	0.32046
5	0.00111	1.34593
6	0.00038	8.87360

Table 6a. Kinetics Parameters for Operating Power (533 K)

Coolant Inlet Temp., K	Effective Delayed Neutron Fraction, β_{eff}	Prompt Neutron Generation Time λ, μs
533	0.00745±0.00021	18.015±0.06

Table 6b. Delayed Neutrons for Operating Power (533 K)

Delayed Neutron Group	Fraction, β_i	Decay Constant, 1/s
1	0.00021	0.01249
2	0.00116	0.03165
3	0.00115	0.11021
4	0.00347	0.32075
5	0.00108	1.34538
6	0.00038	8.89764

Reactivity feedback coefficients were obtained from MCNP calculations at different conditions such as 5% void, or UO2 at elevated temperature, or water moderator in heated channels at elevated temperature. Table 7 lists those conditions and coefficients.

Table 7. Reactivity Calculations

Reactor Conditions	Cold Startup (294 K)	Hot Startup (400 K)	Operating Power (533 K)
Control Rod Location, cm from core axial centerline	-17.907 cm	-15.80	+5.70
Reactivity, k_{eff}	1.00867±0.00010	1.00524±0.00010	1.00790±0.00010
With 5% void	0.99448±0.00010	0.99089±0.00010	0.99488±0.00010
Hot Moderator	1.00941±0.00010 Water at 350 K	1.00533±0.00010	1.00751±0.00010 Water at 600 K vs. 550 K
Doppler	1.00044±0.00010	0.99704±0.00010	0.99518±0.00010
Doppler Feedback Coef., $/K	-0.00343, 294-600 K	-0.00539, 400-600 K	-0.002552, 533-1200 K
Void Coef., $/% void	-0.3637	-0.3796	-0.3486
Water Temp. Coef., $/K	+0.0017, 294-350 K	+0.0002, 400-450 K	-0.0008, 533-600 K

(Transient rod out, control rods positioned to yield approximately 1 $ of reactivity as existed at the time the transient rod was fully ejected from the core.)

Ref. 4, Table II provides the following information listed in Table 8. This table is a mix of measured and calculated values converted to SI units. Presently computed values are also shown in red.

Table 8. Some Experimental [4] and Calculated Neutronic Characteristics

Inlet Temp., K	Peak/avg. power density	Temp. coefficient $/K	Uniform void coefficient $/% void	Doppler coefficient $/K	Reduced prompt neutron generation time ms
294	5.7 4.00, this work	-0.0072 +0.00167, this work	-0.50 -0.3637, this work, core only	-0.01296 [b] -0.00343, this work	2.15 2.28, this work
394	5.2 3.80, this work	-0.036 +0.000235, this work	-0.42 [b] -0.3796, this work, core only	-0.01008 [b] -0.00539, this work	2.18 [b] 2.37, this work
533	3.6 2.89, this work	-0.072 -0.00077, this work	-0.35 [b] -0.3486, this work, core only	-0.00666 [b] -0.00255, this work	2.25 [b] 2.42, this work
533 [a]	3.2 [b]	-0.0738 [b]	-0.37 [b]	-0.00414 [b]	2.25 [b]

[a] at 20 MW; [b] calculated in 1969

In Table 8, the measured temperature coefficient was obtained by uniform heatup of the water in core, reflectors, and all other regions. What is needed for calculating transient response is a temperature coefficient for the core only. That is what was computed.

The reactor core is effectively quite short axially when the control rods are inserted to achieve criticality. Compared with cold, low-power operating conditions, the reactivities required to operate at low power, at 400 K and at 533 K, are enough to require moving the control rods, which in turn causes significant changes in peak to average power, and in radial power shape. The effect of power shape was accounted for, by computing power shapes for the three basic operating conditions of 293 K, 400 K, and 533 K. These shapes were generated with the transient rod fully out of the core, for excess reactivity of the order of +1 $. This was because the average reactivity was close to 1.00 for the 22 tests of interest. Also, it is better to have the power shape closer to the shape after transient rod withdrawal, rather than the critical shape prior to ejection of the transient rod. Significant uncertainty exists because the control rod locations are only provided for the Cold-Startup condition. A very careful computation of feedback effects should account for the spatial variation of the feedback. It is not practical to compute a detailed spatial distribution for a feedback coefficient using a Monte Carlo code. Tallies were created by the MCNP code for axial integrated powers over 20 equal-length axial segments, in the various lumped core regions (universes) shown in Fig.1. A *Mathematica* notebook was created to process the tallies, and to generate a set of normalized axial power shapes, assuming zero power. The normalized power profiles are given in Figs. 4-6. It is suggested that the analysis could be improved by using a diffusion-theory

perturbation code to generate flux-adjoint-weighted worths for each spatial region, of the three feedback coefficients.

SPERT-III Experiments

There were approximately 70 experiments performed. Of these, 15 cases were identified in the Spert III E-Core Reactor Specification to be most significant for analysis for this IAEA work. Seven more cases were also analyzed (see Table 9). Digitized data, taken from published plots giving power and energy, were available from the IAEA for the 17 cases of most interest. It is unfortunate that the published measured data did not include any plots or tables of clad surface temperature vs. time.

Table 9. Cases Analyzed

MEASUREMENTS							
Cold Startup							
Case	Figure	Duration	Reactivity	Tin	Peak Power	Incremental	Clad Surf.
				C		Energy Release	Temp.
		seconds	$		MW	to Peak, MWs	Rise, C
T-18	D-2	7.1	0.9	21	4.3	6.7	55
T-22	D-1	16	0.77	23	2.1	6.9	51
T-41	D-28	0.74	1.13	21	110	3.8	81
T-42	D-29	0.39	1.17	26	170	4.6	82
T-43	D-30	0.29	1.21	26	280	6	82
Hot-Startup							
T-24	D-31	18	0.75	126	3	16	7
T-30	D-35	3.7	0.97	126.1	7.8	4.8	37
T-32	D-43	1.8	1.09	126	66	3.1	57
T-29	D-44	0.98	1.1	126	78	3.2	24
T-70	D-45	0.27	1.21	122	280	6.3	32
T-25	D-32	14.7	0.76	127	2.8	8.9	4.4
T-52	D-47	20	0.64	260	0.14	0.45	0
T-63	D-49	15	0.84	260.6	5.6	15	11.7
T-57	D-55	1.13	1.09	260	89	4.4	17.2
Hot-Standby							
Case	Figure	Duration	Reactivity	Tin	Initial Power	Peak Power	Time of
		seconds	$	C	MW	MW	Peak, s
T-79	D-63	1	0.86	267	1.1	13	0.68
T-80	D-64	1.2	1.08	263	1.3	120	0.15
T-81	D-65	0.24	1.17	262	0.9	330	0.135
T-82	D-67	0.25	1.29	263	1.2	880	0.118
T-83	D-66	0.25	1.25	261	1.1	620	0.117
Operating power							
Case	Figure	Duration	Reactivity	Tin	Initial Power	Peak Power	Time of
		seconds	$	C	MW	MW	Peak, s
T-84	D-68	1.2	0.46	263	19	39	0.18
T-85	D-69	1	0.87	262	19	130	0.155
T-86	D-70	0.5	1.17	261	19	610	0.11

Discussion of Results

Cases T-84, T-85, and T-86: Operating-Power

PARET has numerous simplifications in its fluid model. It is considered to be a conservative, bounding analysis code, not a best-estimate code. During the course of the analysis of all of the tests it became obvious that the feedback effect of fuel heat up (Doppler Effect) was the most significant factor controlling the time evolution of each transient. This same observation was made in SPERT-III documentation. The effect of direct heating was of secondary significant for the hot tests like T-86, but was of much less significance than the Doppler feedback effect. Case T-86 had the largest reactivity insertion, and the highest peak power, of the Operating-Power tests. The coolant temperature coefficient calculated for core only (not reflectors) was very small, but slightly positive at 294 K and at 260 K. At 533 K, it was calculated to be small and negative. This result is similar to that measured, where there was a range where the whole-core temperature coefficient went positive. The void coefficient measured was substantial, but little void was created in most of these tests.

Consequently it was considered appropriate to examine parametrically the measured case with the highest peak power, T-86. The PARET/ANL code was used to "fit" the amount of Doppler feedback ($/K) that would come close to agreement with the measured peak power of Case T-86, while using the MCNP-derived temperature and void feedback coefficients. The result was a peak power of 605.3 MW vs. 610 ± 60 MW measured, using -0.0046 $/K for the fitted Doppler coefficient. The Doppler coefficient derived from the MCNP model calculations was somewhat less: -0.00255 $/K. This same fitted value was then applied to cases T-85 and T-84. The result was a consistent fitted trend in peak power vs. reactivity insertion, shown in Fig.7. The PARET results over-predict the peak power, but they predict the trend of peak power versus reactivity insertion quite well. A similar plot is given in Fig.8 for Hot-Standby tests from 1 MW. Various tables below will show two entries: the nominal or base result, using the MCNP-derived Doppler coefficient, and the "fit" result.

Case T-43, Cold-Startup

The PARET/ANL code was used to study parametrically the amount of Doppler feedback ($/K) that would come close to agreement with the peak power measured for Case T-43. The result was a peak power of 278.7 MW vs. 280 ± 42 MW measured, using a fitted value of- 0.0109 $/K for the Doppler coefficient. The value derived from the MCNP model calculations was much less: - 0.003427 $/K. Without this fit, the peak power was calculated to be 914 MW. This same fitted value was then applied to the other Hot-Startup tests (T-18, T-22, T-41, and T-42). The results were improved as a consequence of using the fitted Doppler feedback coefficient.

Case T-70, Hot-Startup

The PARET/ANL code was used to approximately locate the amount of Doppler feedback ($/K) that would come close to agreement with Case T-70. The result was a peak power of 280.0 MW vs. 280 ± 42 MW measured, using- 0.0115 $/K for the Doppler coefficient. The value derived from the MCNP model calculations was much less: - 0.00539 $/K. Without this fit, the peak power was calculated to be 602 MW. This same fitted value was then applied to the other Hot-Startup tests (T-24, T-30, T-32, T-29, and T-25). The results were improved as a consequence of using the fitted Doppler feedback coefficient.

Results: Cold Startup

Table 10 lists key calculated results for "Cold Startup" cases. They all were initiated from nominally 10 W. Two sets of results are given: "nominal Doppler Feedback" used the feedback coefficient derived from MCNP of -0.00343 $/K, while the "Fitted Doppler Coef." cases required a larger value (in absolute magnitude), of -0.0109 in order to match the peak power of test T-43. The MCNP calculations used the appropriate changes in the S(α,β) data for U in UO_2, and for O in UO_2. Also, the "TMP" cards reflected the required temperature for the fuel meat cells, and the "ZAID" was changed to get the correct temperature continuous-energy cross section libraries for U and O.

Table 10. Cold Startup Cases Analyzed

					Calculated Dopp. Coeff.=-0.00343 $/K			
Cold Startup								
Case	Figure	Duration	Reactivity	Tin	Peak Power	Time of Peak	Energy Release	Clad Surf. Temp.
		seconds	$	C	MW	s	to Peak, MWs	Rise, C
T-18	D-2	7.1	0.9	21	17.69	4.015	17.99	118
T-22	D-1	16	0.77	23	8.769	12.25	23.77	114
T-41	D-28	0.74	1.13	21	393	0.3331	13.11	119
T-42	D-29	0.39	1.17	26	623.7	0.2855	16.34	113
T-43	D-30	0.29	1.21	26	913.7	0.2533	19.61	103
					Fitted Dopp. Coeff.=-0.0109 $/K			(fitted to T-43)
Cold Startup								
Case	Figure	Duration	Reactivity	Tin	Peak Power	Time of Peak	Energy Release	Clad Surf. Temp.
		seconds	$	C	MW	s	to Peak, MWs	Rise, C
T-18	D-2	7.1	0.9	21	5.399	3.706	5.44	111
T-22	D-1	16	0.77	23	2.713	11.5	7.82	108
T-41	D-28	0.74	1.13	21	120.6	0.3136	3.978	110
T-42	D-29	0.39	1.17	26	190.9	0.27	4.934	77
T-43	D-30	0.29	1.21	26	278.7	0.2406	5.933	43.5

Results: Hot Startup

Table 11 lists key calculated results for "Hot Startup" cases. They all were initiated from nominally 10 W. Two sets of results are given: "nominal Doppler Feedback" used the feedback coefficient derived from MCNP of -0.00539 $/K, while the "Fitted Doppler Coef." cases required a larger value (in absolute magnitude), of 0 -0.0115 $/K in order to match the peak power of test T-70. The MCNP calculations used the appropriate changes in the S(α,β) data for U in UO_2, and for O in UO_2. Also, the "TMP" cards reflected the required temperature for the fuel meat cells, and the "ZAID" was changed to get the correct temperature continuous-energy cross section libraries for U and O.

Table 11. Hot Startup Cases Analyzed

Hot Startup				Calculated Dopp. Coeff.=-0.00539 $/K				
Case	Figure	Duration	Reactivity	Tin	Peak Power	Time of Peak	Energy Release	Clad Surf. Temp.
		seconds	$	C	MW	s	to Peak, Mws	Rise, C
T-24	D-31	18	0.75	126	4.652	13.27	13.42	204
T-30	D-35	3.7	0.97	126.1	21.74	1.435	6.298	207
T-32	D-43	1.8	1.09	126	154.5	0.4118	7.171	209
T-29	D-44	0.98	1.1	126	178.8	0.3889	7.619	207
T-70	D-45	0.27	1.21	122	602.5	0.2556	13.29	31.1
T-25	D-32	14.7	0.76	127	4.899	12.459	13.4	167
Hot Startup				Fitted Dopp. Coef. =-0.0115 $/K		(fitted to T-70)		
Case	Figure	Duration	Reactivity	Tin	Peak Power	Time of Peak	Energy Release	Clad Surf. Temp.
		seconds	$	C	MW	s	to Peak, Mws	Rise, C
T-24	D-31	18	0.75	126	2.396	12.87	7.353	149
T-30	D-35	3.7	0.97	126.1	10.14	1.362	2.922	191
T-32	D-43	1.8	1.09	126	72.09	0.3946	3.333	201
T-29	D-44	0.98	1.1	126	83.31	0.373	3.538	146
T-70	D-45	0.27	1.21	122	280	0.2472	6.165	20.6
T-25	D-32	14.7	0.76	127	2.512	12.08	7.286	99

Results: Hot-Standby

Table 12 lists key calculated results for "Hot-Standby" cases. They all were initiated from nominally 1 MW. Two sets of results are given: "nominal Doppler Feedback" used the feedback coefficient derived from MCNP of -0.00255 $/K, while the "Fitted Doppler Coef." cases required a larger value (in absolute magnitude), of 0 -0.0046 $/K in order to match the peak power of test T-86. The MCNP calculations used the appropriate changes in the S(α,β) data for U in UO_2, and for O in UO_2. Also, the "TMP" cards reflected the required temperature for the fuel meat cells, and the "ZAID" was changed to get the correct temperature continuous-energy cross section libraries for U and O.

Table 12. Hot Standby Cases Analyzed

Hot-Standby									
					Calculated Dopp. Coeff.=-0.00255 $/K				
Case	Figure	Duration	Reactivity	Tin	Initial Power	Peak Power	Time of Peak	Energy Release	Clad Surf. Temp.
		seconds	$	C	MW	MW	s	to Peak, MWs	Rise, C
T-79	D-63	1	0.86	267	1.1	18.58	none	n.a.	33
T-80	D-64	1.2	1.08	263	1.3	197.7	0.152	7.988	51
T-81	D-65	0.24	1.17	261	0.9	581.9	0.1409	14.72	56
T-82	D-67	0.25	1.29	262.5	1.2	1592	0.1248	25.31	54
T-83	D-66	0.25	1.25	261	1.1	1199	0.1287	21.72	55
Hot-Standby									
					Fitted Dopp. Coef.=-0.0046 $/K (fitted to T-86)				
Case	Figure	Duration	Reactivity	Tin	Initial Power	Peak Power	Time of Peak	Energy Release	Clad Surf. Temp.
		seconds	$	C	MW	MW	s	to Peak, MWs	Rise, C
T-79	D-63	1	0.86	267	1.1	13.89	2.305	24.73	26
T-80	D-64	1.2	1.08	263	1.3	148.8	0.1448	5.847	39
T-81	D-65	0.24	1.17	261	0.9	405.9	0.1362	10.25	55
T-82	D-67	0.25	1.29	262.5	1.2	1069	0.1218	17.15	53
T-83	D-66	0.25	1.25	261	1.1	812.6	0.1253	14.85	54

Results: Operating Power

Table 13 lists key calculated results for "Operating Power" cases. They all were initiated from 19 MW. Two sets of results are given: "nominal Doppler Feedback" used the feedback coefficient derived from MCNP of -0.00255 $/K, while the "Fitted Doppler Coef." cases required a larger value (in absolute magnitude), of 0 -0.0046 $/K in order to match the peak power of test T-86. The MCNP calculations used the appropriate changes in the S(α,β) data for U in UO_2, and for O in UO_2. Also, the "TMP" cards reflected the required temperature for the fuel meat cells, and the "ZAID" was changed to get the correct temperature continuous-energy cross section libraries for U and O.

Table 13. Operating Power Cases Analyzed

Operating Power									
						Calculated Dopp. Coeff.=-0.00255 $/K			
Case	Figure	Duration	Reactivity	Tin	Initial Power	Peak Power	Time of Peak	Energy Release	Clad Surf. Temp.
		seconds	$	C	MW	MW	s	to Peak, MWs	Rise, C
T-84	D-68	1.2	0.46	262.5	19	35.35	0.0991	1.233	48
T-85	D-69	1	0.87	261	19	122.7	0.0905	3.869	55
T-86	D-70	0.5	1.17	261	19	840.4	0.1014	17.18	108
Operating Power									
						Fitted Dopp. Coef.=-0.0046 $/K (fitted to T-86)			
Case	Figure	Duration	Reactivity	Tin	Initial Power	Peak Power	Time of Peak	Energy Release	Clad Surf. Temp.
		seconds	$	C	MW	MW	s	to Peak, MWs	Rise, C
T-84	D-68	1.2	0.46	262.5	19	34.92	0.0766	0.8566	48
T-85	D-69	1	0.87	261	19	113.9	0.0852	3.2	54
T-86	D-70	0.5	1.17	261	19	610.3	0.098	12.44	58

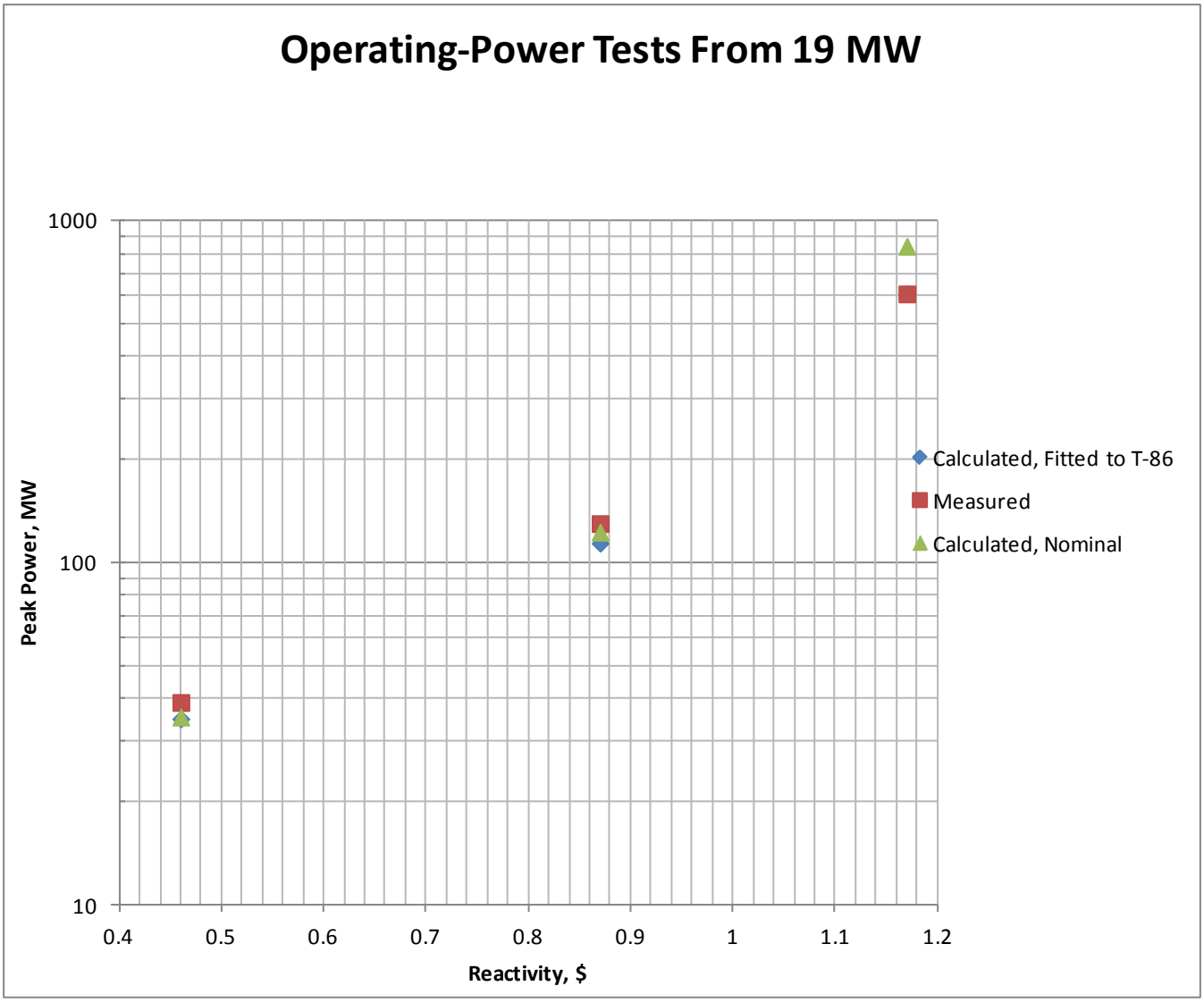

Fig.7. Operating-Power Tests from 19 MW

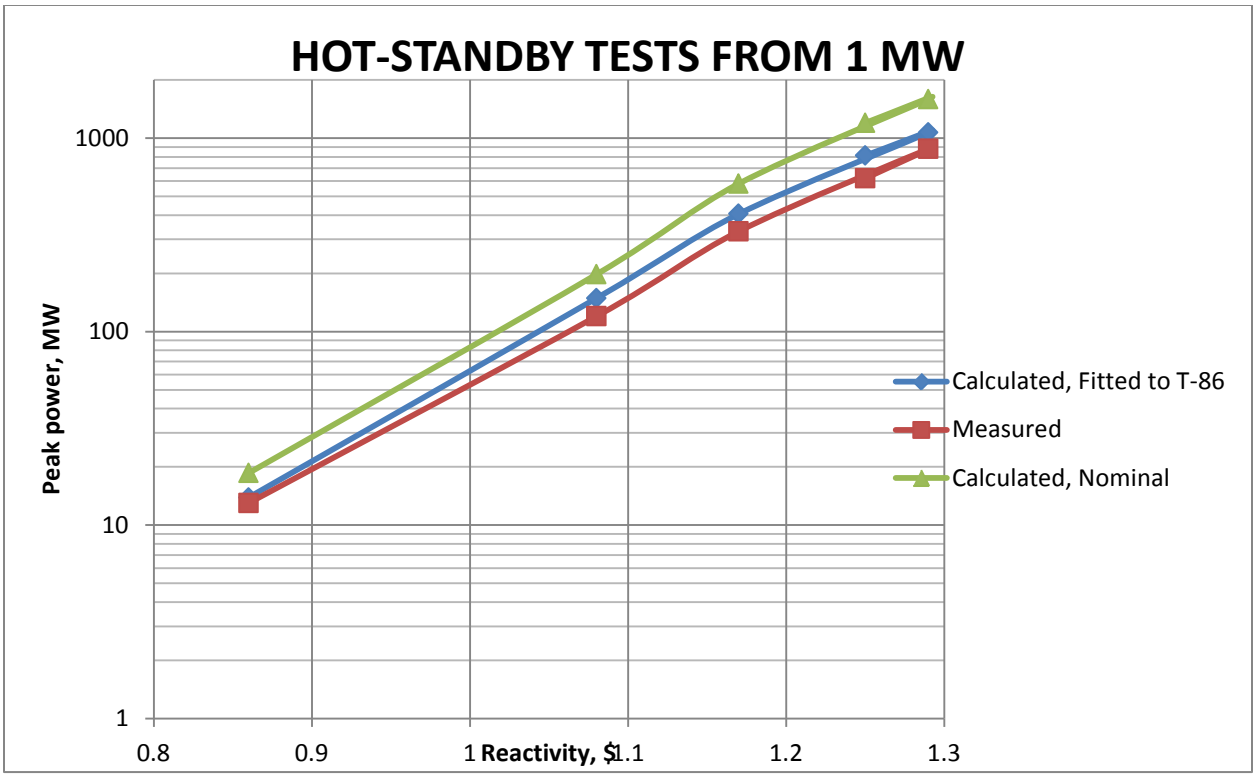

Fig.8. Hot-Standby Tests from 1 MW

Results: Cold Startup

Case T-18

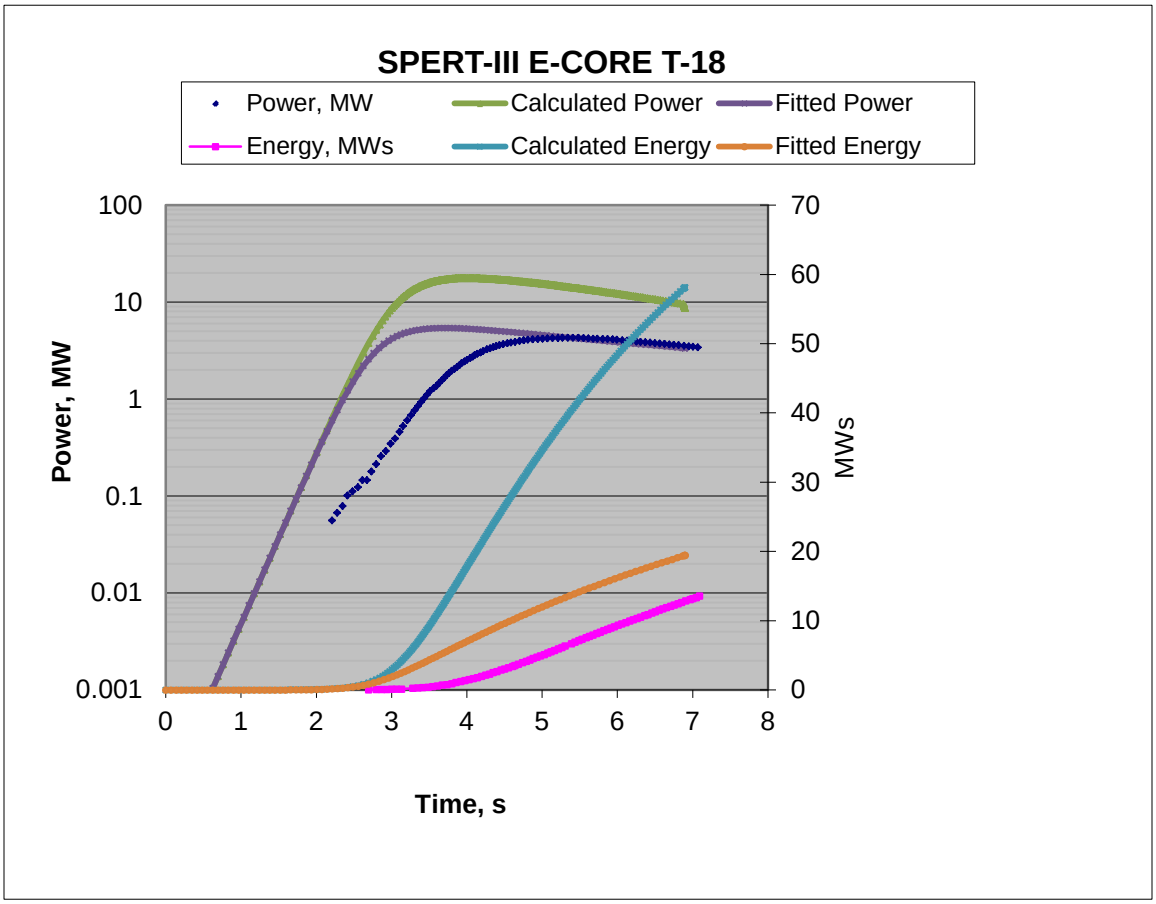

Fig.9. SPERT-III E-CORE, Test T-18: Evolution of Power and Energy Release

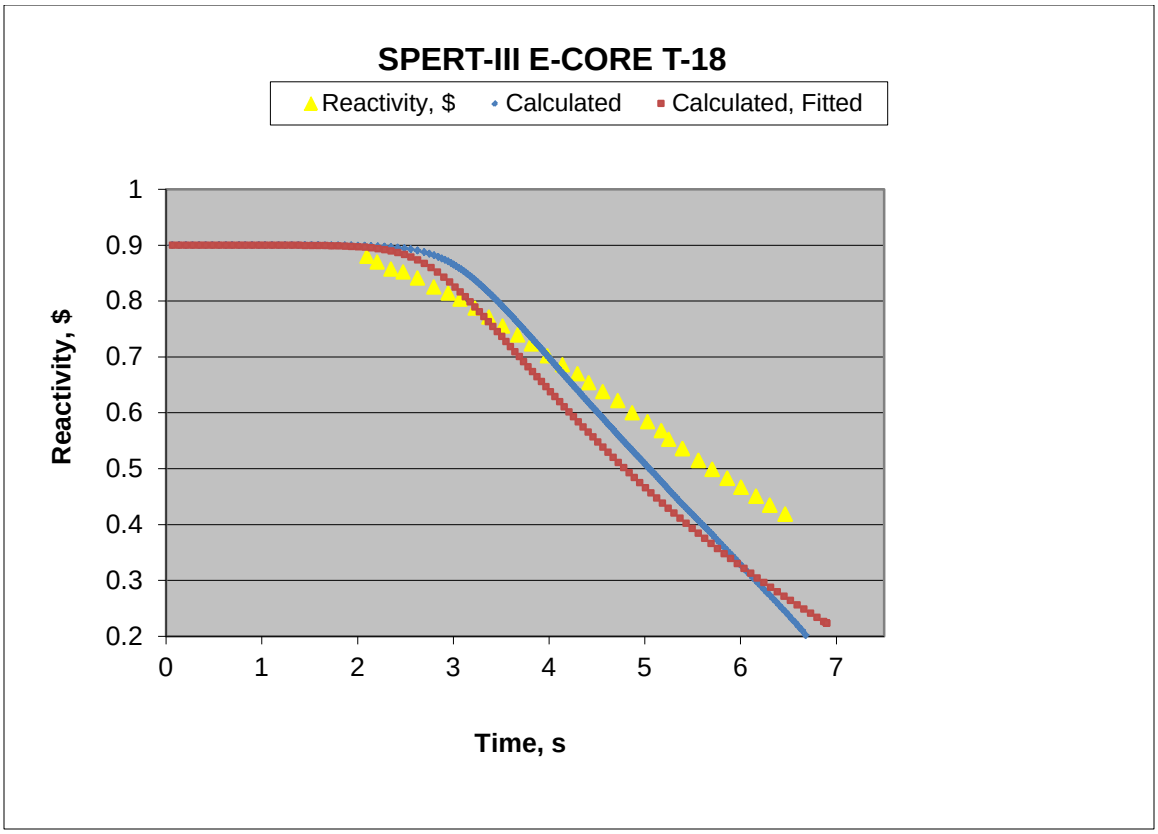

Fig.10. SPERT-III E-CORE, Test T-18: Evolution of Reactivity

Case T-22

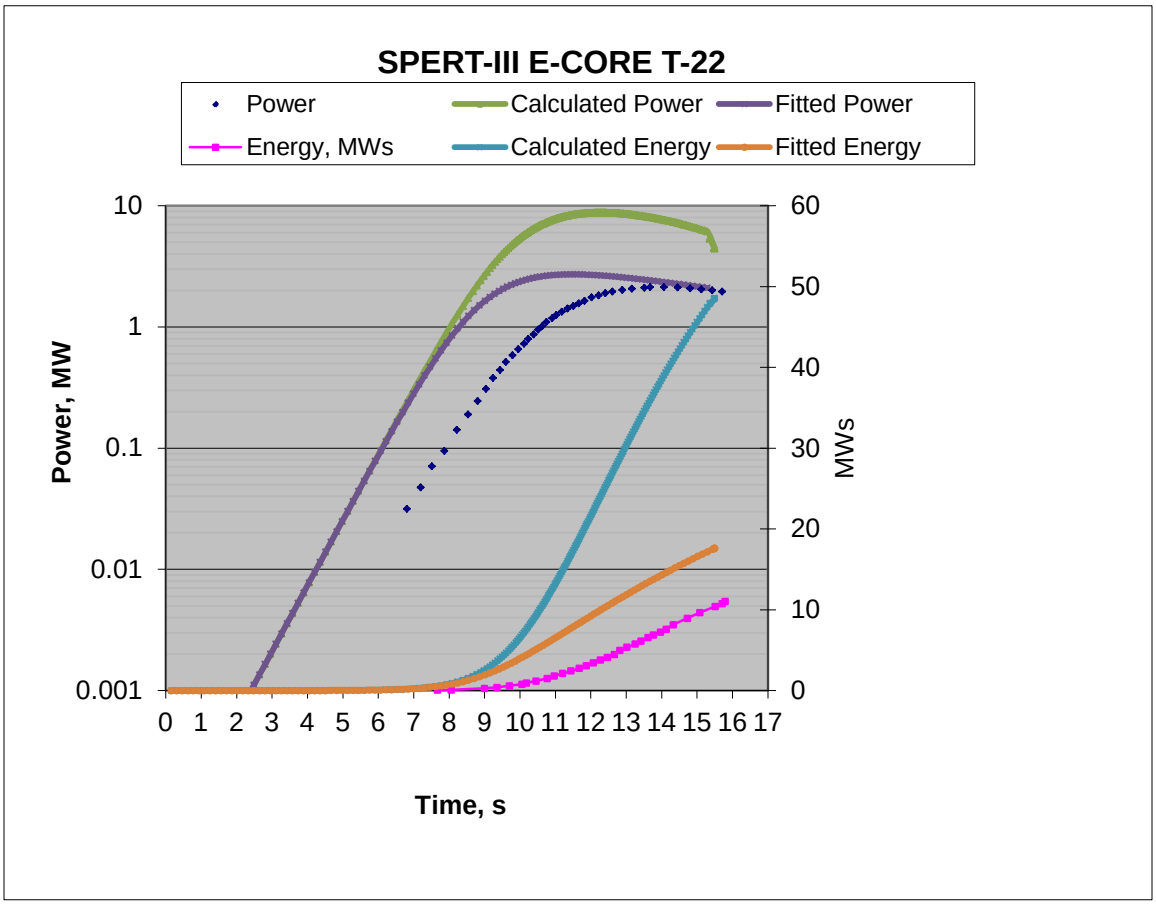

Fig.11. SPERT-III E-CORE, Test T-22: Evolution of Power and Energy Release

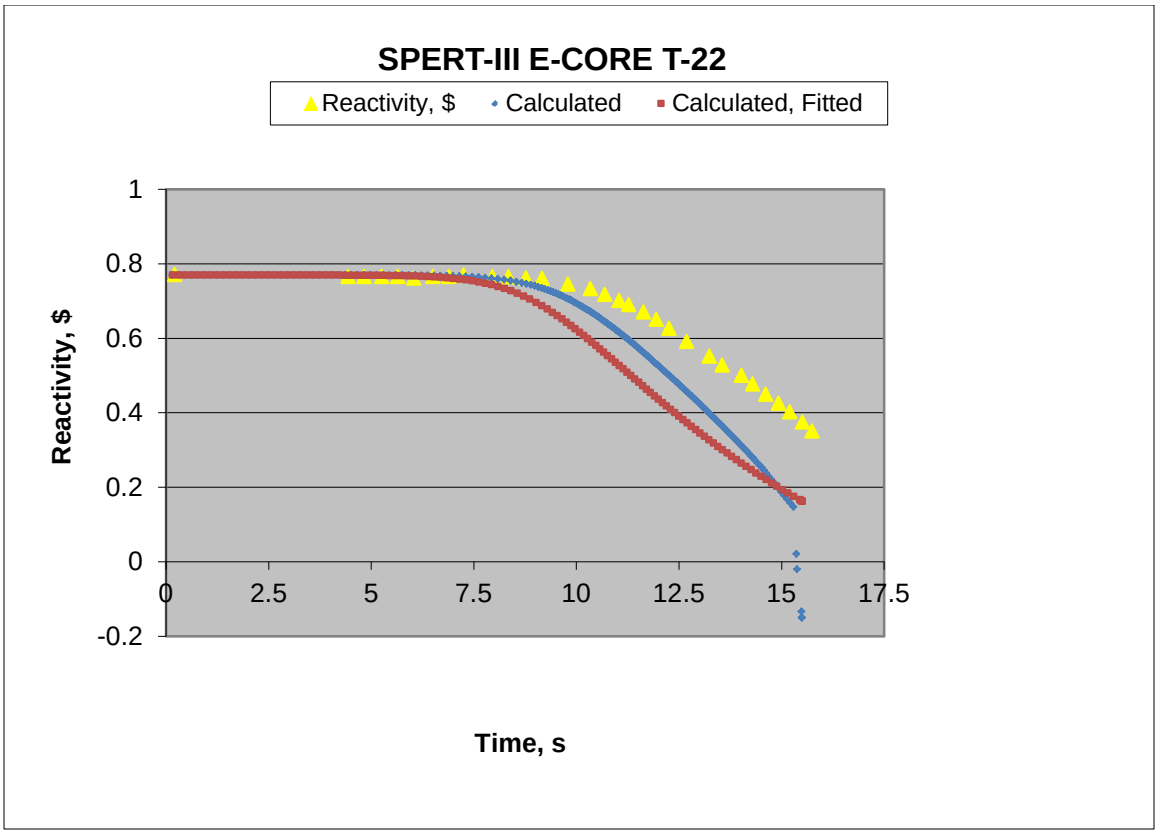

Fig.12. SPERT-III E-CORE, Test T-22: Evolution of Reactivity

Case T-43

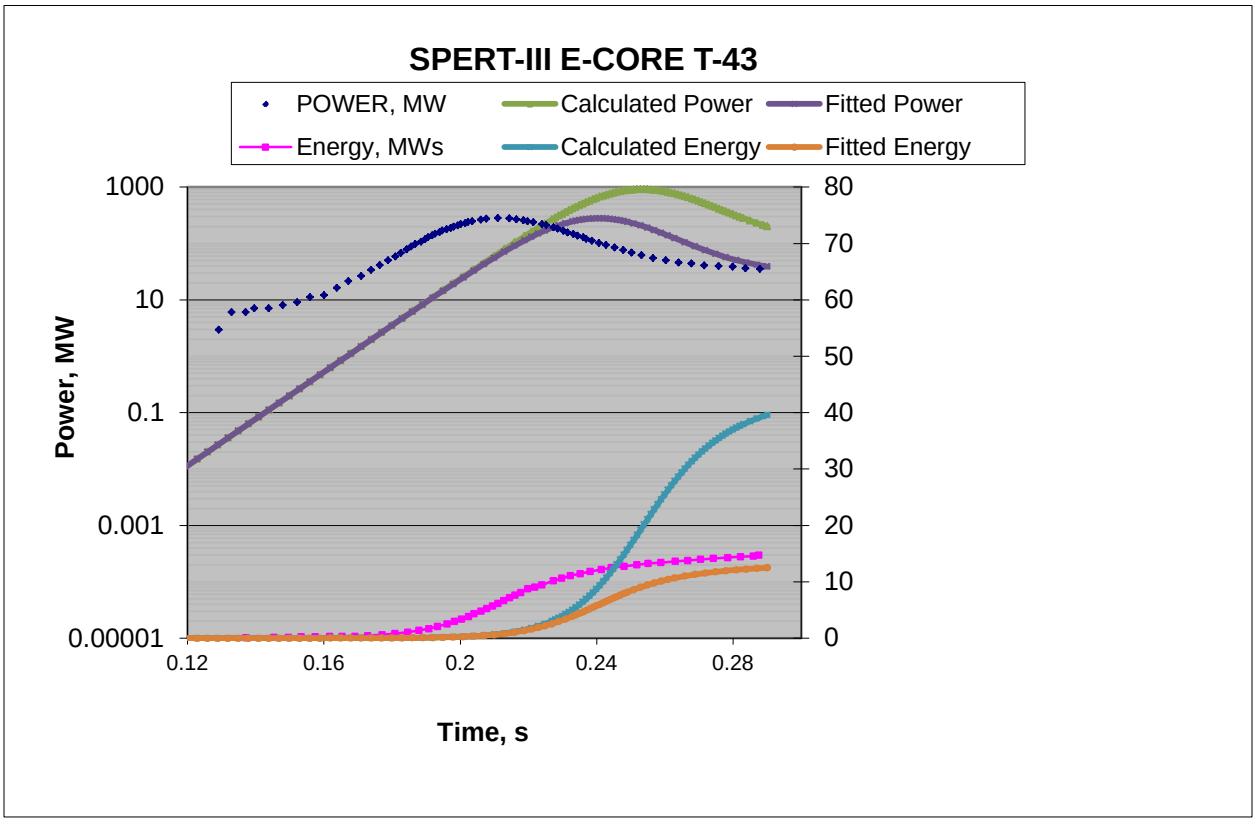

Fig.13. SPERT-III E-CORE, Test T-43: Evolution of Power and Energy Release

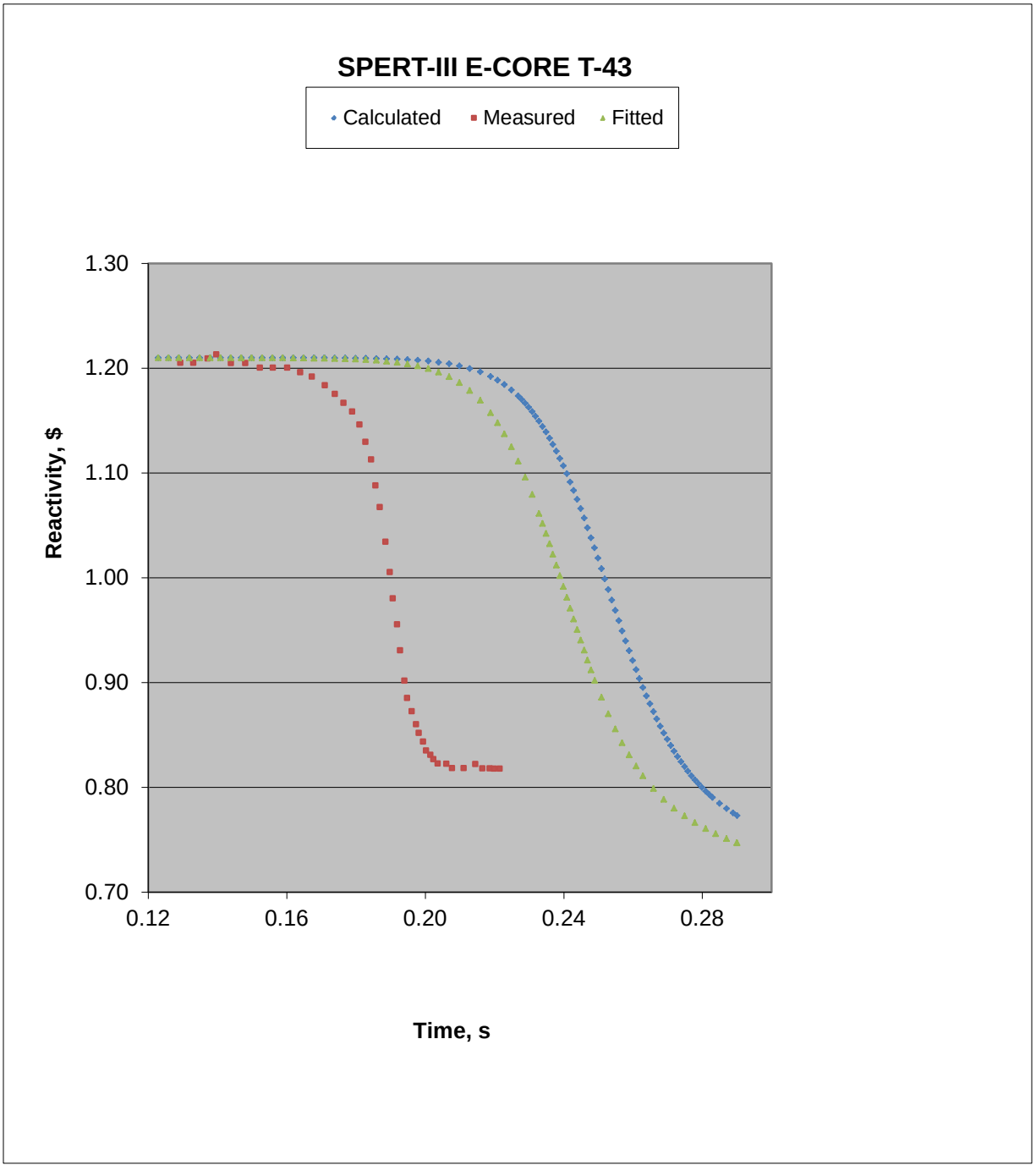

Fig.14. SPERT-III E-CORE, Test T-43: Evolution of Reactivity

Case T-70

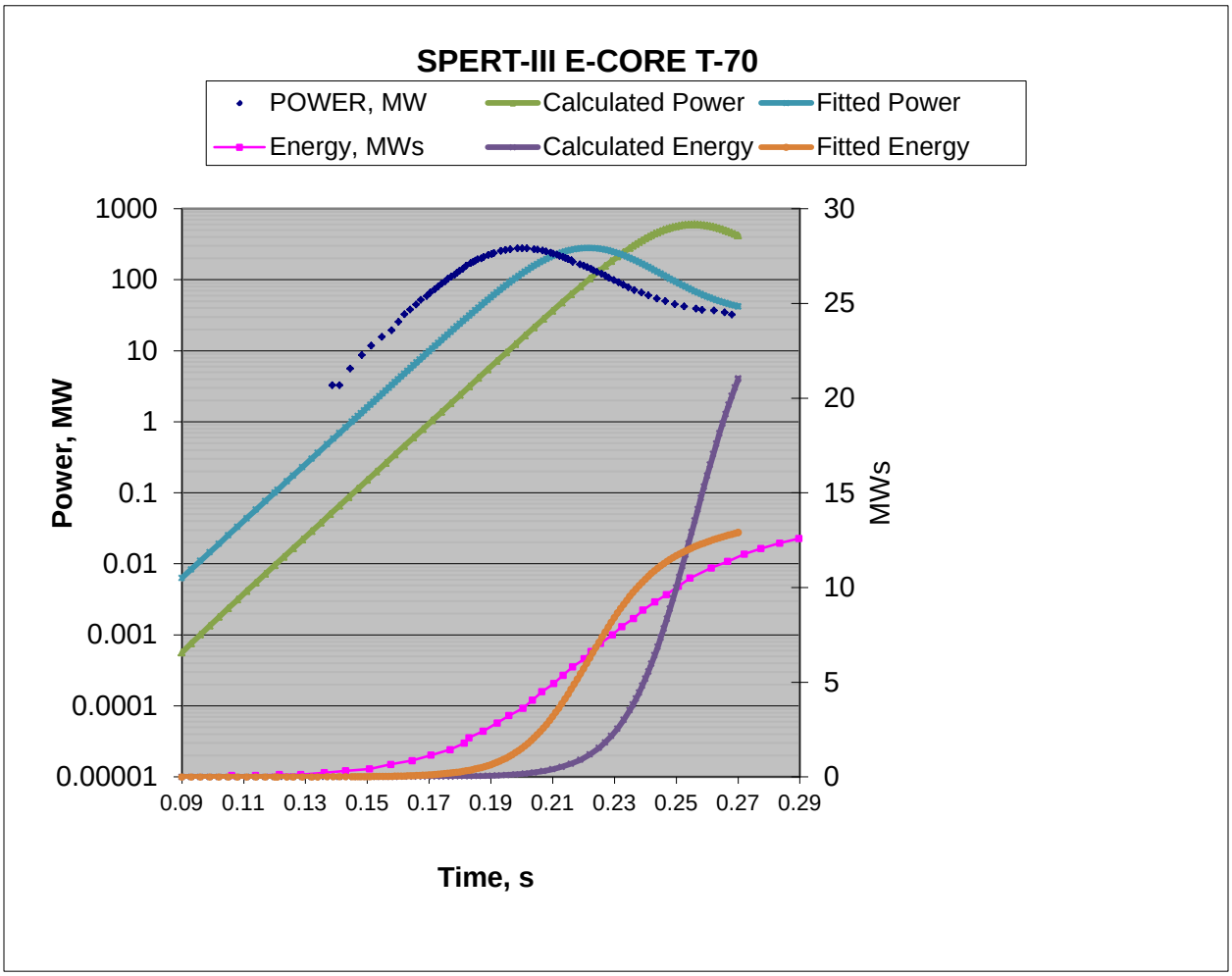

Fig.15. SPERT-III E-CORE, Test T-70: Evolution of Power and Energy Release

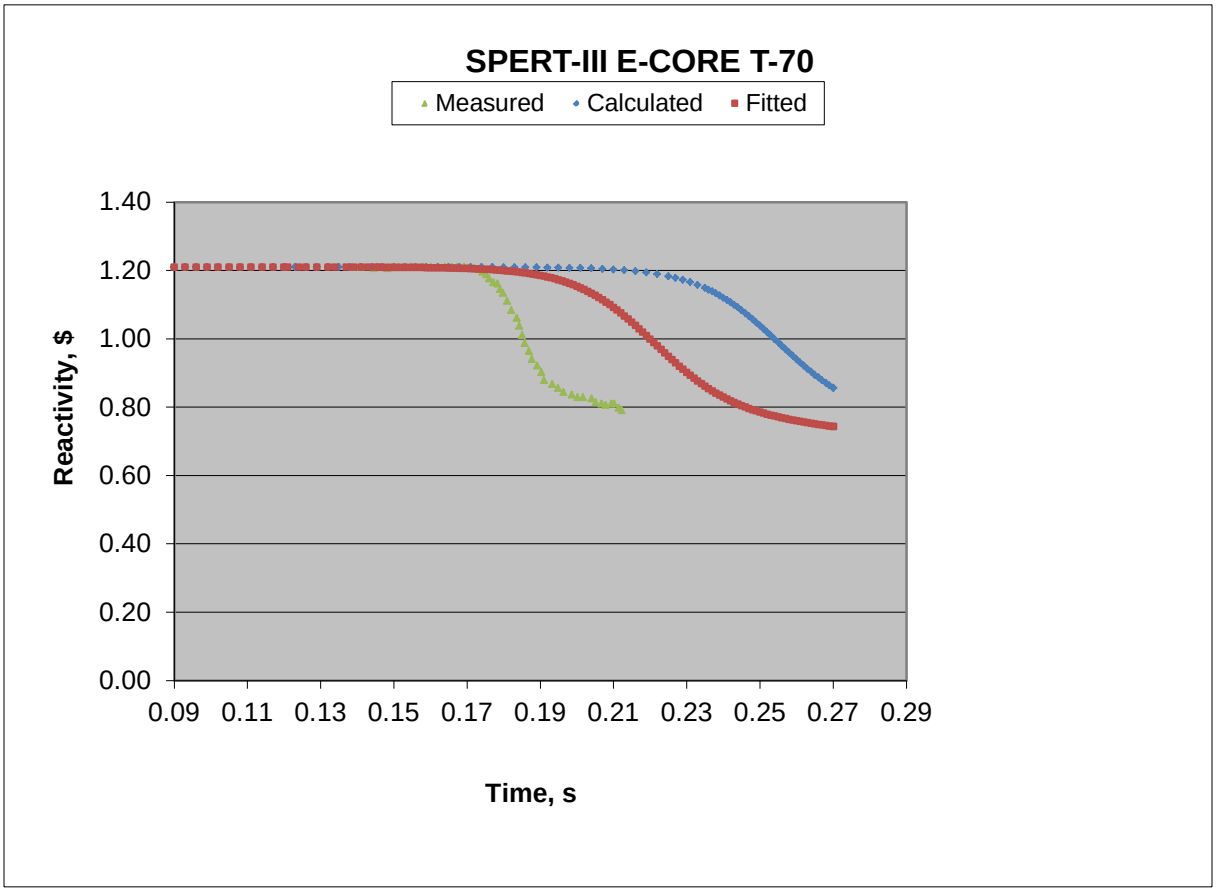

Fig.16. SPERT-III E-CORE, Test T-70: Evolution of Reactivity

Case T-86

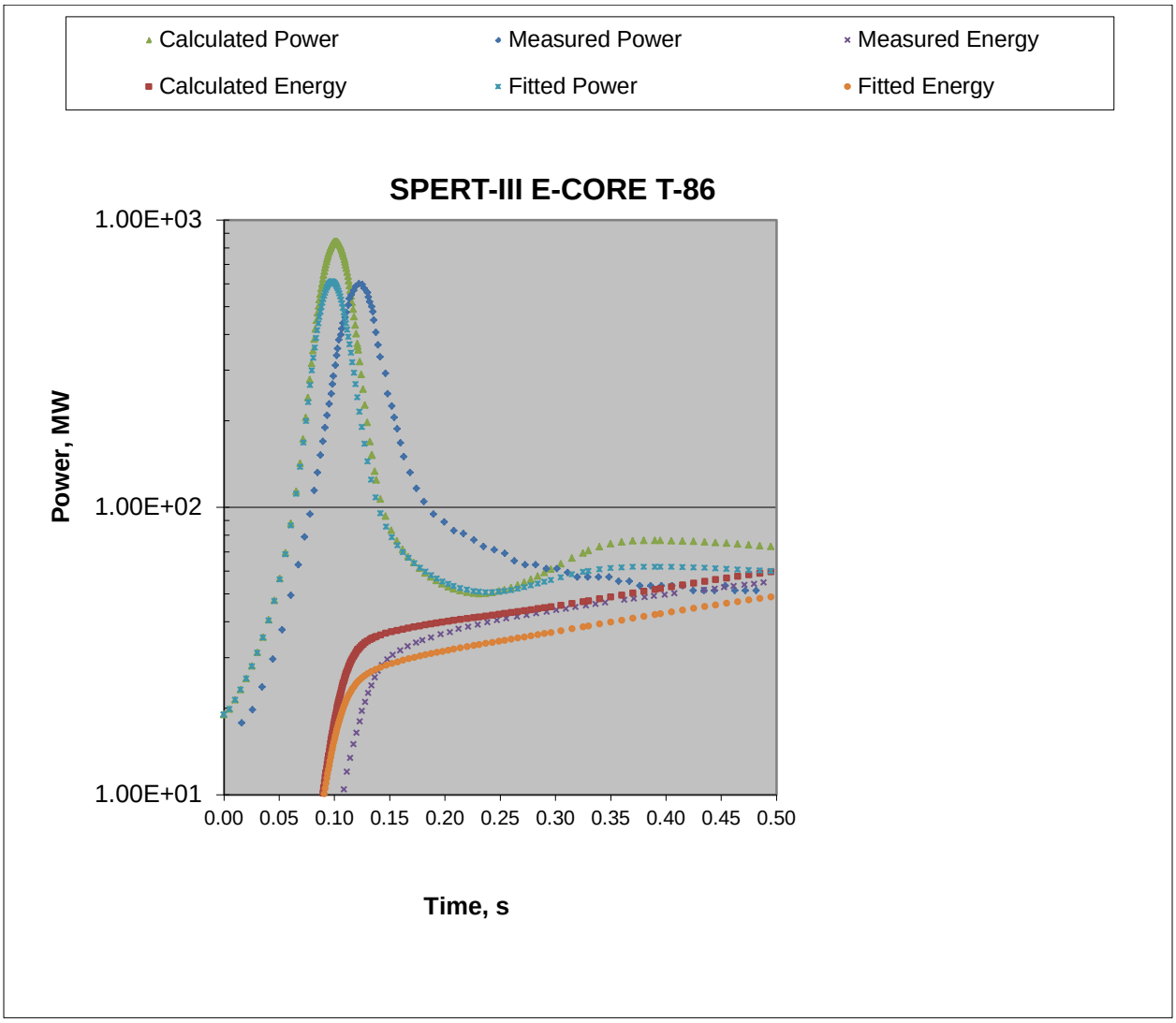

Fig.17. SPERT-III E-CORE, Test T-86: Evolution of Power and Energy Release

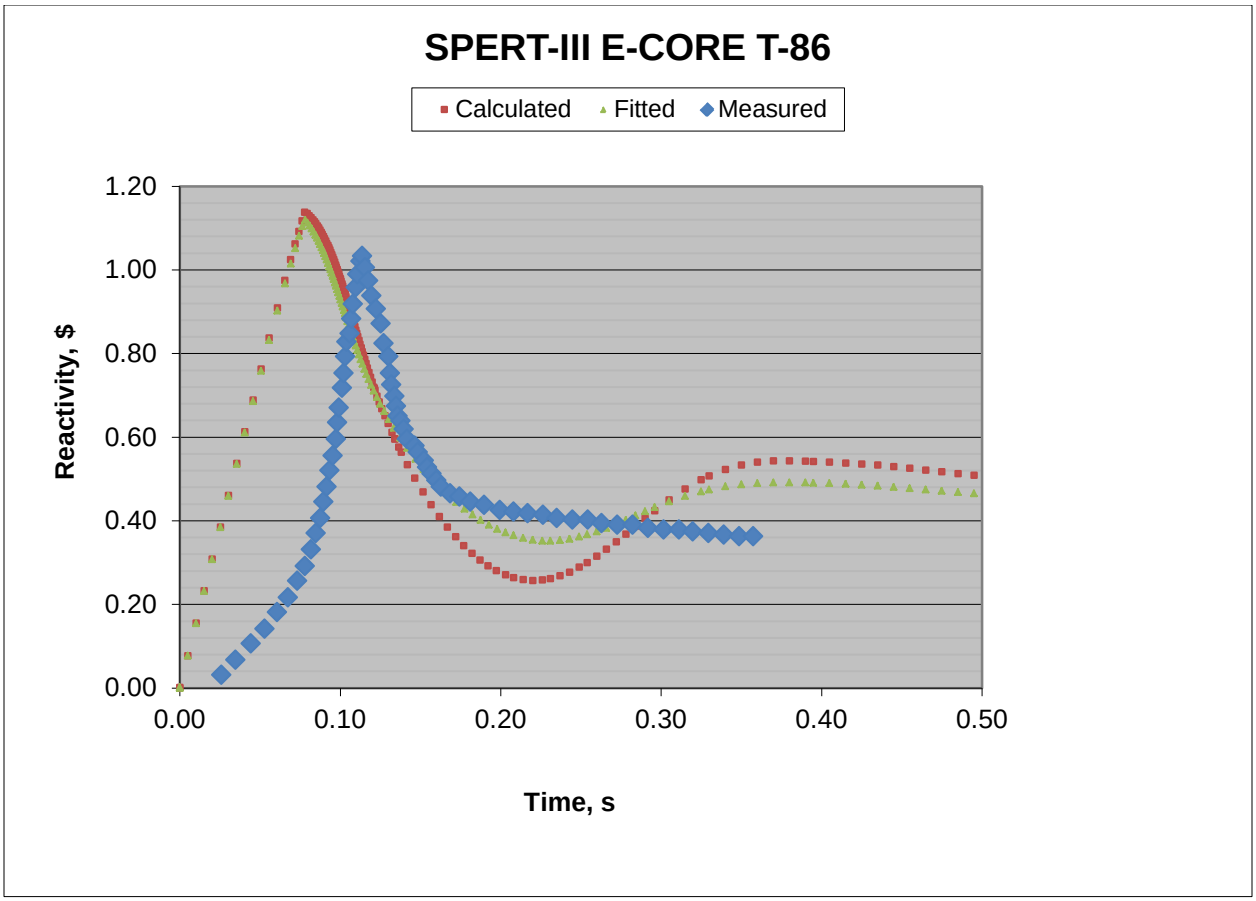

Fig.18. SPERT-III E-CORE, Test T-86: Evolution of Reactivity

Discussion of Results Concerning Reactivity Feedback, and Clad Surface Temperature Rise

There is some uncertainty as to the initial power of each test. One can see that typical calculations of power (for example, cases T-18, T-22, and T-43 plotted in Figs. 9, 11, and 13) show about the same slope, indicating that the period is correct, but that there may be a time offset caused by this uncertainty in initial power (for example, case T-70 in Fig. 15, which shows a time offset of about 25 ms). In addition, there is quite a large uncertainty on the reactivity insertion. Key results for peak power and peak clad surface temperature are very sensitive to plus or minus one standard deviation (4 %) on reactivity insertion. As a result, it may have been better to fit the reactivity to the measured reactor period because its standard deviation is 2%.

It is noted that the PARET results are always conservative: they predict too high a peak power, and too high an energy release. This leads to predicting too high a temperature rise in the clad. But one can also observe from Figs. 7 and 8 that the trends in power vs. reactivity are excellent.

Calculated temperature coefficients are limited in accuracy by statistical uncertainties. Calculated values in Table 8 are listed as small and positive for 294 K and for 400 K, but are within one standard deviation of zero. The value for 533 K is small and negative, with a standard deviation of ±19%. Fortunately, the temperature feedback is very much less than either of the void and Doppler feedbacks.

Table 14 lists a comparison between experiment and calculation for most of the tests of reactivity feedback at peak power. For Example, Cold Startup Case T-22 had a measured (deduced) reactivity compensation at peak power of 0.26±0.03 $, while PARET (nominal Doppler feedback) showed 0.268 $ total of which 0.267 $ was Doppler. As a second example, Cold Startup Case T-43 had a measured (deduced) reactivity compensation at peak power of 0.22±0.02 $, while PARET (nominal Doppler feedback) showed 0.231 $ total of which 0.231 $ was Doppler. It is concluded that reactivity compensation at peak power compares well with estimates made in Reference [4].

A related issue is whether or not boiling takes place. The majority of the experiments experienced no measured boiling (see Table 15 and Figs. 19-22). Now consider the calculations, for the nominal Doppler feedback coefficient. A close inspection of Fig.9 for T-18, and Fig.11 for T-22, will show a sharp reduction in calculated power at the very end of the test. This is caused by the onset of significant boiling. One can also see that the use of the fitted Doppler coefficient shows no dip, and has no boiling.

Clearly, the Doppler Effect from heat-up of the UO_2 dominates the shape of each test power vs. time curve. There is so little temperature rise in the low-power tests that there is no void production, and the temperature coefficient for the water is quite small.

Table 15 is similar to Table 14, but lists a comparison between measured and calculated clad surface temperature rise. This comparison is somewhat flawed in that the measurement was taken along an outer rod of the 4x4 transient fuel section—therefore with the transient rod out—which may not be quite the same as computed. The PARET code reports the absolute maximum detected in the course of

the event, which may be different than in the 4x4 fuel of the transient rod assembly. Another difference is due to the fact that the axial power shape and peak value in the calculations is very sensitive to the position of the control rods. It is concluded that the Cold-Startup tests, which had no flow at the start of each transient, is seriously over-predicted. The other test conditions with flow also over-predict, but appear to be more reasonable.

It is worth noting that a smaller plate-type core, called the SPERT III-C 19/52 core, had many similar tests conducted with it [11]. This core was fully-enriched uranium oxide in stainless steel clad. The results of those tests included temperature versus time plots, which are not available for the E-core of concern for this work.

Table 14. Reactivity Compensation at Peak Power

Case	Reactivity Compensation at Peak Power, $ (measured)	Reactivity Compensation at Peak Power, $ (calculated)	Reactivity Compensation at Peak Power, $ (fitted)
Cold-Startup			Fitted to T-43
T-18	0.23±0.03	0.188	0.188
T-22	0.26±0.03	0.268	0.284
T-41	0.14±0.01	0.157	0.154
T-42	0.18±0.02	0.193	0.189
T-43	0.22±0.02	0.231	0.229
Hot-Startup			Fitted to T-70
T-24	0.35±0.04	0.213	0.202
T-30	0.15±0.02	0.260	0.275
T-32	0.11±0.01	0.126	0.129
T-29	0.12±0.01	0.136	0.127
T-70	0.22±0.02	0.236	0.231
T-25	0.22±0.02	0.258	0.272
T-52	0.06±0.01	n.a.	n.a.
T-63	0.29±0.03	n.a.	n.a.
T-57	0.12±0.01	0.125	0.130
Hot-Standby			Fitted to T-86
T-79	0.09	No peak	0.187
T-80	0.11	0.116	0.117
T-81	0.18	0.192	0.192
T-82	0.26	0.306	0.305
T-83	0.30	0.266	0.267
Operating-Power			Fitted to T-86
T-84	0.03	0.003	0.003
T-85	0.04	0.040	0.049
T-86	0.22	0.208	0.216

Table 15. Clad Surface Temperature Rise

Case	Measured Clad Surf. Temp. Rise, K	Calculated Clad Surf. Temp. Rise, K	Fitted Clad Surf. Temp. Rise, K
Cold Startup			
T-18	55 ± 5	118	111
T-22	51 ± 5	114	108
T-41	81 ± 8	119	110
T-42	82 ± 8	113	77
T-43	82 ± 8	103	43.5
Hot-Startup			
T-24	7 ± 0.6	204	149
T-30	37 ± 4	207	191
T-32	57 ± 6	209	201
T-29	24 ± 2	207	146
T-70	32 ± 3	31	21
T-25	4 ± 0.6	167	99
T-52	≈0	1.6	1.5
T-63	12 ± 1	39	28
T-57	17 ± 1	46	34
Hot-Standby			
T-79	0 ± 6	33	26
T-80	13 ± 6	51	39
T-81	20 ± 6	56	55
T-82	25 ± 6	54	53
T-83	20 ± 6	55	54
Operating-Power			
T-84	47 ± 6	48	48
T-85	48 ± 6	55	54
T-86	54 ± 6	108	58

Comparison of Predictions of Peak Clad Surface Temperature

Table 15 and Figs. 19-22 compare predictions of peak clad surface temperature rise (that is, the change relative to the initial conditions prior to the transient) with measurement. The measured values are shown with statistical uncertainties of ± 1 standard deviation by the “Lower” and “Upper” bars in the charts.

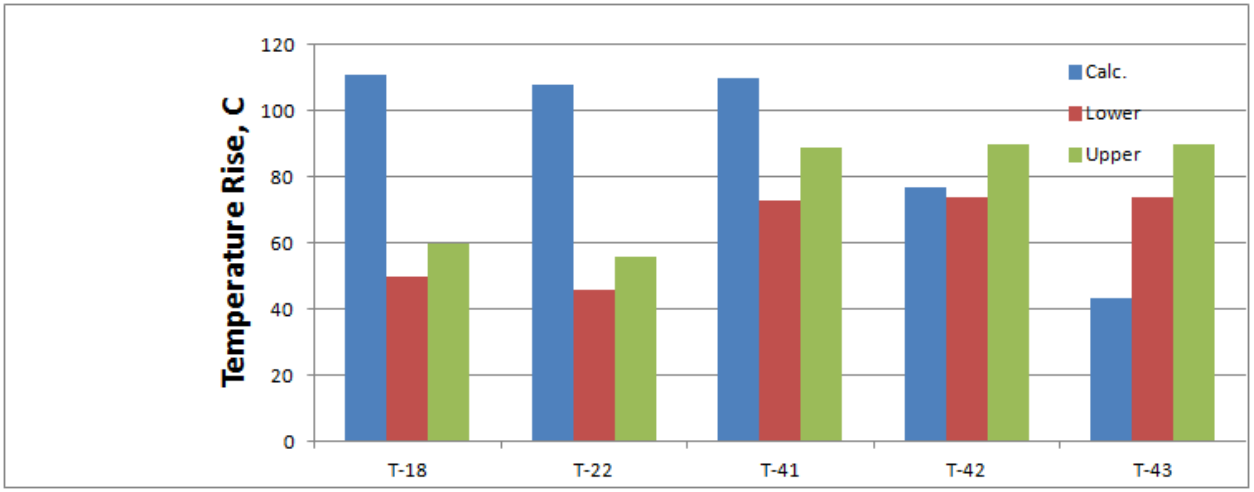

Fig.19. Comparison of Predictions of Peak Clad Surface Temperature Rise (T-18, T-22, T-41, T-42, T-43), 294 K, Zero Initial Flow, Cold Startup

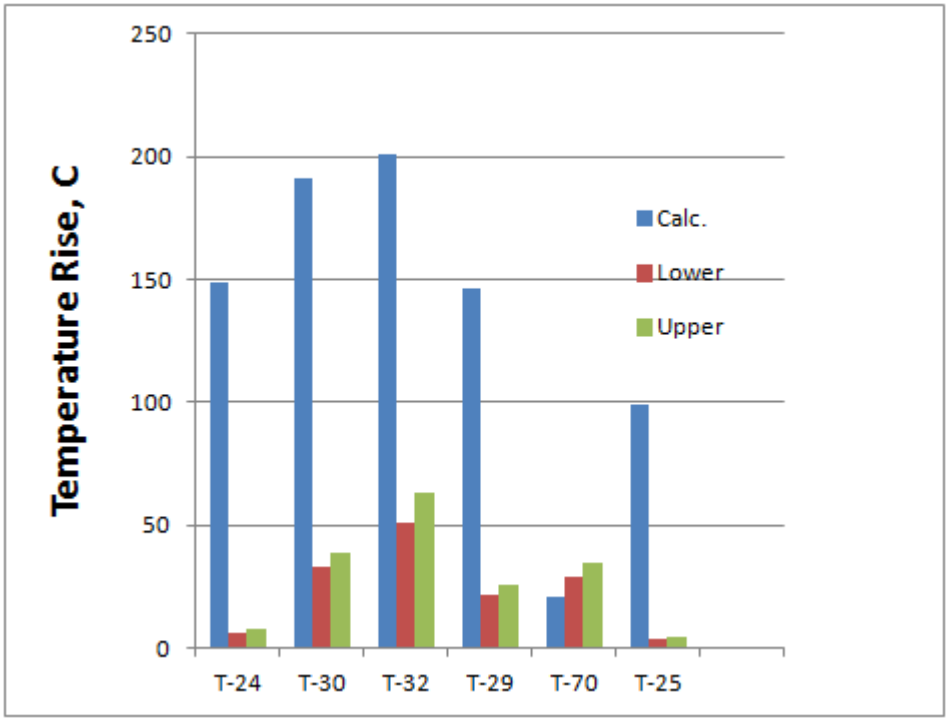

Fig.20. Comparison of Predictions of Peak Clad Surface Temperature Rise (T-24, T-30, T-32, T-29, T-70, T-25), 400 K, Hot Startup, With Flow

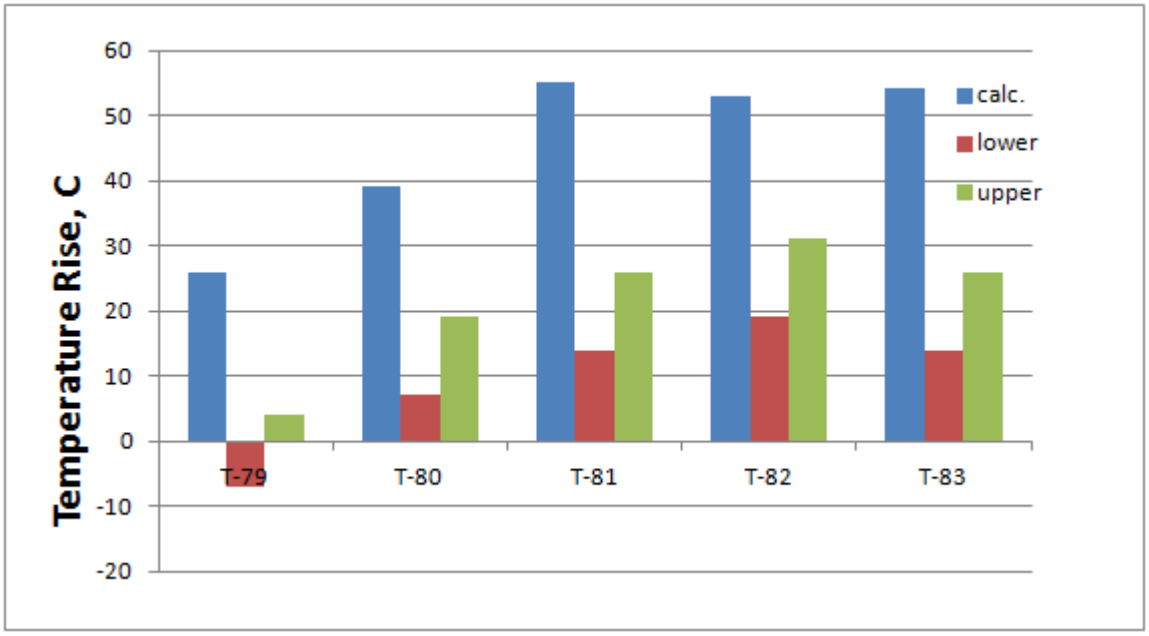

Fig.21. Comparison of Predictions of Peak Clad Surface Temperature Rise (T-79, T-80, T-81, T-82, T-83), 533 K, Hot Standby, With Flow

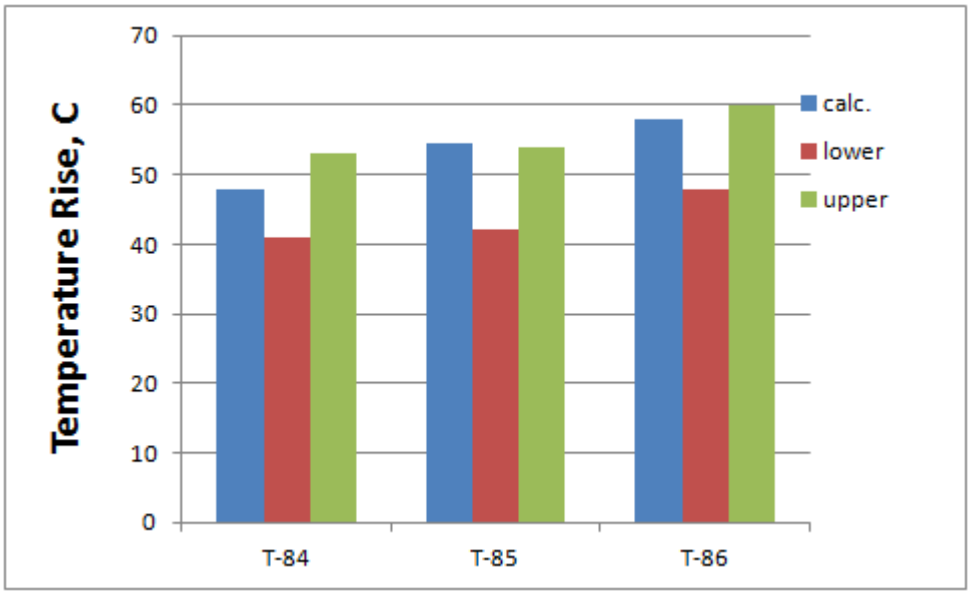

Fig.22. Comparison of Predictions of Peak Clad Surface Temperature Rise (T-84, T-85, T-86), 533 K, Operating Power, With Flow

Control Rod Worth vs. Position

Control rod reactivity calculations were performed for 294, 400, and 533 K. The transient rod is fully out, with the steel follower in the core. The operational sequence before any transient test is as follows. As an example, assume that the test is to be performed for a rapid insertion of 1.20 $. This will be accomplished by pre-positioning the transient rod to introduce -1.20$, and by making the reactor critical by removing the control rods just enough to introduce +1.20 $ of reactivity. Then, given that the reactor is running at critical at a power of a few watts, the transient rod absorber is rapidly expelled from the reactor core. At the end of the transient rod expulsion, the reactor is super-prompt critical with a reactivity of +1.20 $.

The results shown in Fig.23 assume that the transient rod absorber section is fully out (the steel follower is fully in). This is the configuration of the core in every test, after the desired reactivity insertion is attained by rapidly ejecting the transient rod. The values of β_{eff} used are given in Tables 4a, 5a, and 6a. The results for 294 and 400 K are very close together (the feedbacks provide a reactivity change of about 2 $ between 294 and 400 K).

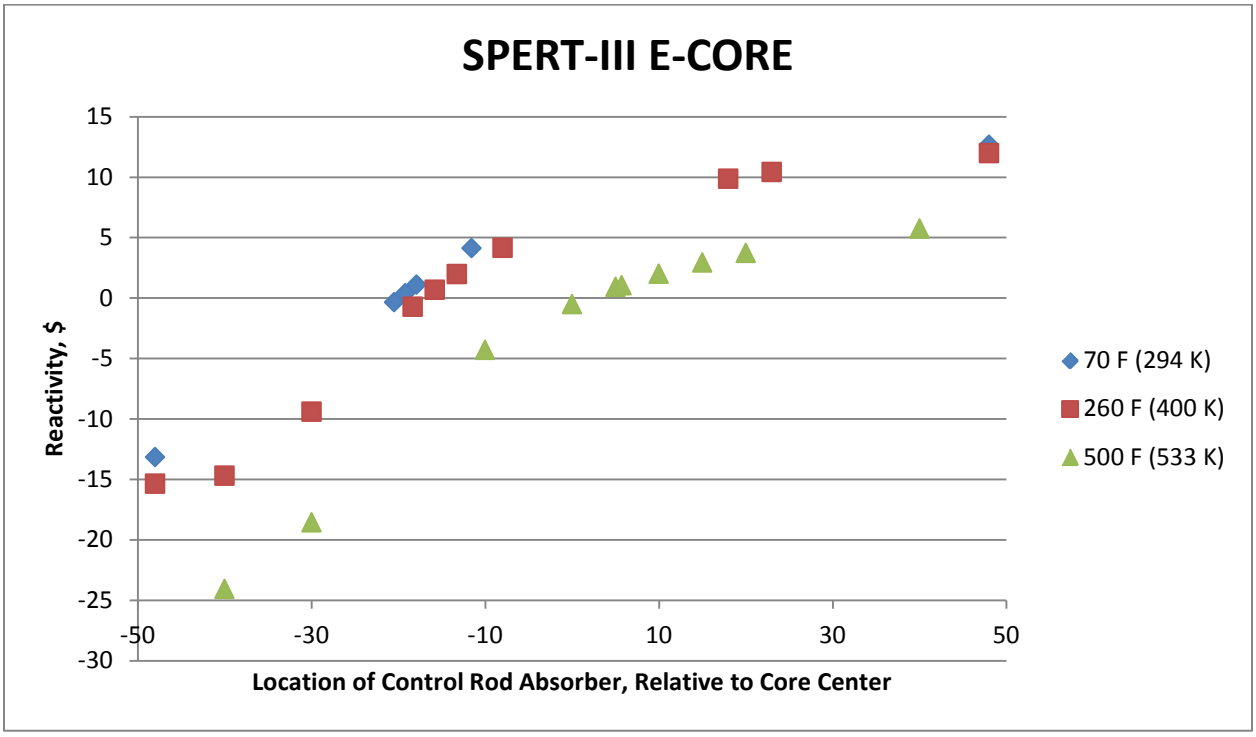

Fig.23. Control Rod Reactivity Worth vs. Position

Recommendations for Future Work

Section 8 of Ref. [12] addresses reactivity insertion rates caused by rapid ejection of the transient rod at a design acceleration of 50.8 m/sec/sec. Given the reactivity change with position for the transient rod, with its worth set to zero when the reactor is critical just prior to ejection, it is possible to deduce a curve of reactivity worth vs. time after initiating ejection of the transient rod. One can make the simplifying assumption that the reactivity insertion rate can be modeled as a 15 $/s ramp, as was done here. For events beginning at high power (1-19 MW), it was recommended in [12] that a more realistic shape to the reactivity vs. time curve be used.

Fig.24 shows an approximate set of transient rod worth curves as functions of time after initiating transient rod ejection, from low power at 533 K. The curves are not smooth due in part to statistical uncertainties in the derived reactivities for small changes in the rod position, and because more axial locations are needed to better define the curves. One can see that using a fixed insertion rate of 15 $/s is about right for a desired insertion of 1 $, but it is too slow for insertions > 1$, and too fast for insertions < 1 $. As a result, one can expect a shift in time for the power peak, between measurements and calculations. Curves similar to Fig.24 could be obtained for the other temperature conditions of interest at 294 K and at 400 K.

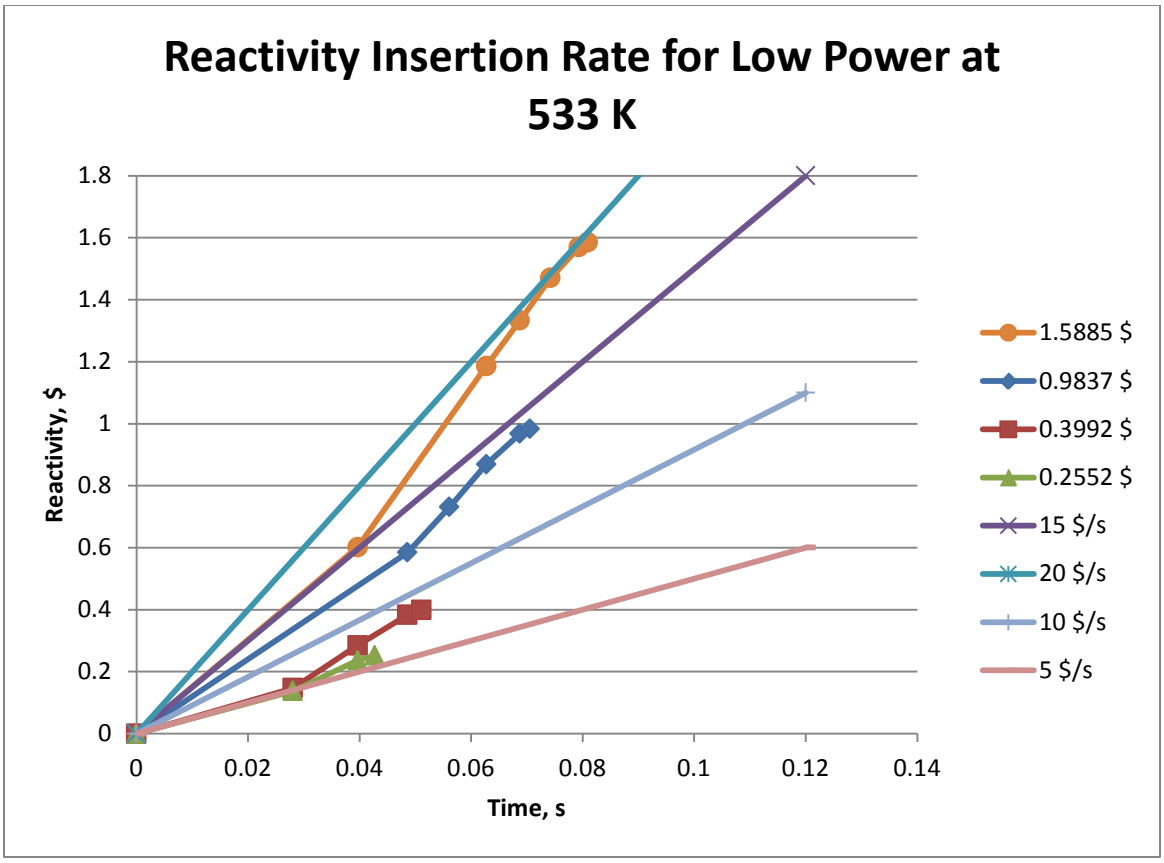

Fig.24. Transient Rod Reactivity Worth vs. Time, for Low-Power Operation at 533 K

A few experimental tests at 533 K were re-calculated to ascertain the effect of introducing the reactivity as two ramps, based on Fig.24. Tests T-52, T-57, T-84, and T-86 were selected. Table 16 provides the results. It can be seen that only case T-86 shows a significant change in the power peak. There is a trend to shift the power peak later, as expected. Finally, there is essentially no change in clad surface temperature rise. Similar tests at Cold Startup conditions should be investigated in future.

Table 16.The Effect of Reactivity Insertion as a Double Ramp Instead of a Single Ramp at 15 $/s

	T-52	T-57	T-84	T-86
Reactivity, $	0.64	1.09	0.46	1.17
Ramp Rates, $/s	9.70, then 11.0	13, then 20	5, then 12.3	12, then 19.09
Shift in Power Peak, %	-0.58	0.0	0.22	8.0
Time shift of Power Peak, ms	0	0.6	12.9	2.6
Shift in Clad Surface Temp. Rise, C	0.01	0.0	0.01	0.02

Member states of the Nuclear Energy Agency may wish to locate [13], which the author was unable to obtain because the USA is not a Member State. This document seems to describe a reactor benchmark configuration for SPERT-III for the companion plate-type core. If so, it could provide more information regarding design details for the control rods and transient rod in the E-core because they could be very similar.

ACKNOWLEDGEMENTS

Work supported by the U. S. Department of Energy National Nuclear Security Administration Under Contract No. DE-AC02-06CH11357.

References

1. X-5 Monte Carlo Team, LA-UR003-1987, MCNP— A General Monte Carlo N-Particle Transport Code, Version 5, Volume I: Overview and Theory, April 24, 2003 (Revised 2/1/2008).

2. A. P. Olson, A Users Guide to the PARET/ANL Code, ANL/RERTR/TM-11-38, Version 7.5, June 1, 2011.

3. J. Dugone, Editor, SPERT III REACTOR FACILITY: E-CORE REVISION, AEC Research and Development Report, IDO-17036, Nov. 1965.

4. R. K. McCardell, D. I. Herborn, and J. E. Houghtaling, REACTIVITY ACCIDENT TEST RESULTS AND ANALYSES FOR THE SPERT Ill E-CORE -- A SMALL, OXIDE-FUELED, PRESSURIZED-WATER REACTOR, IDO-17281, TID-4500, March 1969.

5. Shigeaki Aoki, Takayuki Suemura, Junto Ogawa and Toshikazu Takeda, Analysis of the SPERT-III E-Core Using ANCK Code with the Chord Weighting Method, Journal of NUCLEAR SCIENCE and TECHNOLOGY, Vol. 46, No. 3, p. 239–251 (2009).

6. Clad specifications were obtained from: 1989 SAE Handbook vol.1 for 347 ss, p. 10.124.

7. The lower and upper grid specifications were taken from: R. E. Heffner and T. R. Wilson, SPERT-III REACTOR FACILITY, IDO-16721, AEC Research and Development Report, TID-4500, October 25, 1961, p. 24.

8. http://asm.matweb.com was the source for type 304 or 304L stainless steel composition.

9. Lead brick shielding was assumed to conform to ASTM B29 Specification (2011).

10. Flow calculations were reported in IDO-16416 (Quarterly Progress Report, July, August, September, 1957. Reactor Projects Branch, Edited by G. O. Bright, Ed. 13, October 1, 1957).

11. R. Scott, Jr., C. L. Hall and R. N. Hagen ,Tests of the Fully Enriched Uranium Oxide Stainless Steel Plate-Type C-Core in the SPERT Ill E-CORE REACTOR: Data Summary Report, IDO-17223, TID-4500, February 1967.

12. R. K. McCardell, D. I. Herborn, and J. E. Houghtaling, Reactivity Accident Test Results for the SPERT III E-Core—a Small, Oxide Fueled, Pressurized-Water Core, Report IDO-17281, TID-4500, March 1969.

13. Report NEA/NSC/DOC/(95)03 II, Volume II, HEU-COMP-THERM-022, “SPERT III STAINLESS-STEEL-CLAD PLATE-TYPE FUEL IN WATER,” Soon S. Kim, INNEL (date unknown).

Nuclear Engineering Division
Argonne National Laboratory
9700 South Cass Avenue, Bldg. 208
Argonne, IL 60439-4842

www.anl.gov

Argonne National Laboratory is a U.S. Department of Energy laboratory managed by UChicago Argonne, LLC